

BRNO UNIVERSITY OF TECHNOLOGY
FACULTY OF CIVIL ENGINEERING

Dr.techn. Ing. Jan Podroužek

**SPATIAL MATERIALS FOR ADDITIVE
MANUFACTURING**

HABILITATION THESIS

Brno 2019

Technology is a word that describes something that doesn't work yet.

Douglas Adams.

Preface

This monograph was conceived as an overview of conducted theoretical and experimental research relating to the concept of construction 4.0, exploring the new design possibilities and challenges stemming from large-scale layer based 3D printing, where structural members no longer have to be limited to rectilinear and solid bodies, and where manufacturing complexity is free, unlike in traditional manufacturing process. The results of multi-scale approach in the design optimization, typically yielding organic streamlined structures with bio-inspired infill patterns, may thus be fabricated without extreme costs.

This topic emerged over time due to my involvement at both Institute of computer aided engineering and computer science and Institute of structural mechanics, and advanced as I had the opportunity to develop a large scale 3D printing laboratory at the research center for advanced materials and structures (AdMaS). Presented manuscript also partially utilizes already published papers by the author. All presented figures, unless otherwise stated, are created or generated by the author himself.

As a main applicant, the author also acknowledges the funding from the Technology Agency of the Czech Republic, supporting the ongoing applied research project *Vacuum coating system for rapid prototyping*.

I am grateful to all current and former colleagues, PhD students and graduate students from the Brno University of Technology, University of Natural Resources and Life Sciences, Vienna, and Vienna University of Technology, who have somehow contributed to this thesis, for instance, by being involved in theoretical discussions, 3D printing of specimens, experimental testing etc.

I reserve my deepest gratitude for my family, for their support, encouragement and forbearance.

I hope you enjoy your reading.

Jan Podroužek
Brno 2019

Contents

1	Introduction	13
I	Additive manufacturing technology	17
2	Construction 4.0	19
2.1	Additive manufacturing process	19
2.1.1	Vat Photopolymerization (VP)	20
2.1.2	Material Jetting (MJ)	20
2.1.3	Binder Jetting (BJ)	20
2.1.4	Material Extrusion (ME)	21
2.1.5	Powder Bed Fusion (PBF)	21
2.1.6	Sheet Lamination (SL)	21
2.1.7	Direct Energy Deposition (DED)	21
2.2	Robotic arm systems	21
2.3	Gantry systems	22
2.4	Small robots printing large-scale structures	22
2.5	Cable-driven robots	22
3	Structural scale applications	25
3.1	Concrete	26
3.2	Adobe	27
3.3	Polymers	27
4	Collaborative research	29
II	Generative design	35
5	Motivation by topology optimization	37
5.1	Transition to branching structures	38
5.2	Generated organic structures	40
6	Multi-scale optimization	45
7	Periodic minimal surfaces	51
7.1	RVE characterization	53

III Spatial materials	59
8 3D infill patterns	61
8.1 Gyroid	61
8.2 Schwarz surfaces	62
9 Experimental investigation	65
9.1 Production of specimens	65
9.2 Physical tests	68
10 Results	81
10.0.1 Experimental	81
10.0.2 Numerical	82
10.0.3 Vacuum coating	85
11 Discussion	89
12 Conclusion and outlook	91

Chapter 1

Introduction

Throughout history, architecture was influenced by technology. Gothic arches and vaults made it possible to bring buildings much higher than before. Steel frames and elevators made it possible to bring them even higher as first skyscrapers were built. Last century has seen the introduction of Computer Aided Design (CAD), the last major leap in construction technologies. Since then architecture hasn't seen many game-changing technologies and robotics may well be the next one.

By integrating the computational design and digital fabrication process, the additive manufacturing (AM) has developed over the last decades into various forms, providing architects and designers with efficient tools for rapid prototyping, individualisation and low-volume production. Conventional AM methods include stereolithography (SLA), fused-deposition modeling (FDM), and selective laser sintering (SLS), as implemented in a number of commercial 3D printing systems. As AM has become accessible, the complexity of the geometry is no longer a constraint, as will be shown in this thesis, where the layer-based FDM method is utilized.

Although 3D printing is traditionally utilized for rapid prototyping and for high-value, low-volume production, such as in the aerospace industry, the last years have seen many successful efforts in upscaling the 3D printing systems to structural and architectural scales. Most of such large scale 3D printing systems are, however, still to be considered rather experimental. This also applies to autonomous construction systems in general, where autonomous and self-sufficient robots perform not only the 3D printing, but also manipulation or excavation tasks [21].

When compared to the proposed autonomous construction systems, the traditional fabrication technology in civil engineering can be considered slow, labour intensive, dangerous, expensive, and constrained to primarily rectilinear forms, often resulting in homogenous structures. The associated annual fatalities is estimated to 50,000, which amounts to 17% of all workplace accidents.

The shift to autonomous construction systems could potentially improve safety, speed, and quality. Furthermore, this technology enables the operation in inhospitable, extreme or extra-terrestrial environments, such as arctic environments or those caused by natural disasters. The extra-terrestrial application of autonomous and self-sufficient 3D printing is considered to be the primary construction technique involved in the colonization of Mars [19] or Moon [6]. It is also believed, that autonomous construction systems could easily adapt to site-specific conditions and constraints and, thus, contribute to sustainable construction in general.

By accepting 3D printing as part of the future of civil engineering and construction, the multi-scale optimization of structures, i.e. the outer shape of the structure and the inner configuration of materials (or infills), becomes quite desirable as the geometrical complexity of both no longer represents an obstacle. For example, some of the presented structural

patterns (3D infills) cannot be manufactured by conventional approaches, such as extrusion or moulding, with the exception of weaving, which is, however, limited only to several periodic minimal surfaces and scales beyond practical use in structural engineering.

The 1st RILEM International Conference on Concrete and Digital Fabrication (2018) is another indicator showing the growing interest of the concrete community in AM with cementitious materials.

Possible applications in the near future may include on-site 3D printing of entire structures or structural members, or prefabrication of structural members or small structures. In terms of successful applications of large scale 3D printing or robotic fabrications, new experimental realizations emerge more and more often both from academia and industry, such as the contributions from IAAC (see e.g. [16]), the autonomous construction rig from MIT [21] or the 100 square meter house 3D printed in cement for the Milan Design Week 2018 (CLS Architetti), to name the very few.

From a structural point of view an interesting alternative to the layer-based 3D printing is the stress line additive manufacturing (SLAM), which has been proposed recently by [43]. The deposition of filaments along the principal stress lines improves the anisotropic limitation of the conventional layer-based FDM, but may require more forming material (supports).

Layer based 3D printing at architectural scales with cementitious materials or straw reinforced mud is implicitly considered in the following discussions and motivations, while the experimental campaign and mechanical characterization is based on small-scale layer-based FDM using PLA (polylactic acid). Note that the current market with 3D printing filaments offers stronger materials than PLA, such as Polycarbonate (40% higher tensile strength). However, the purpose of this study was not an optimization of load carrying capacity but instead to investigate the potential of different infill patterns. The author believe that some of the principles and results stemming from the small scale campaign will be generally valid and valuable for the consequent design of real-scale experiments with structural materials, such as concrete.

After introducing the background of topological optimization and the infill options considering the technological constraints of 3D printing, an experimental campaign aiming at a quantification of infill options in terms of load capacity / weight ratio and stiffness / weight ratio is presented. Finally, the results are generalized utilizing elastic finite element analysis. All presented figures are based on results generated by authors.

The aim of the presented thesis is to introduce and characterize, both experimentally and numerically, several classes of non-traditional 3D infill patterns at various scales as an alternative to classical 2D infill patterns in the context of additive manufacturing and structural applications.

The investigated 3D infill patterns are biologically inspired and include Gyroid, Schwarz D and Schwarz P. Their selection was based on their beneficial mechanical properties, such as double curvature, are not only known from nature but also emerge from numerical topology optimization. A classical 2D hexagonal pattern has been used as a reference. Mechanical performance of 14 cylindrical specimens in compression is quantitatively related to stiffness, peak load and weight. Digital image correlation provides accurate full-field deformation measurements and insights into periodic features of the surface strain field. The associated variability, which is inherent to the production and testing process, has been evaluated for 3 identical Gyroid specimens. The nonlinear material model for the preliminary FEM analysis is based on tensile test specimens with 3 different slicing strategies. The 3D infill patterns are generally useful when the extrusion orientation cannot be aligned with the build orientation and

the principal stress field, i.e. in case of generative design, such as the presented branching structure, or any complex shape and boundary condition.

The thesis is divided into three successive parts. The first introduces the additive manufacturing technology in general, reviews the current advancements related to construction industry and describes the technical infrastructure which has been utilized by the author during the presented investigation.

The second part introduces the general aspects of generative design, multi-scale optimization and periodic minimal surfaces, and presents examples of organic streamlined structures with bio-inspired infill patterns.

The third part presents the 3D infill patterns as an alternative to classical 2D patterns and discuss the results of the experimental campaign.

Part I

Additive manufacturing technology

Chapter 2

Construction 4.0

The "fourth industrial revolution", or industry 4.0 concerns digitalisation and virtualization of Industry, in general. The "Construction 4.0" is a branch of Industry 4.0 and refers to the digitalisation and virtualization of the construction industry. Although BIM (Building Information Modelling, Building Information Model or Building Information Management) is traditionally considered central to Construction 4.0, as well as increased implementation of machine learning (ML), artificial intelligence (AI), drones, sensors and predictive analytics, this thesis is oriented towards robotic manufacturing at structural or architectural scales, optionally on-site and autonomous, also referred to as 3D printing, additive manufacturing (AM) or digital manufacturing (DM).

Note that DM is more general than AM and is not limited to FDM (Fused Deposition Modeling) or paste extrusion, and may include robotic manipulation, formatting (cutting, drilling) and deposition (chemically or mechanically bonded) of existing members, such as wooden beams (Figure 2.1) or bricks.

FDM (also known as Fused filament fabrication, FFF) works on the additive principle by depositing thermoplastic filament along a predetermined path and is commonly used for prototyping but rarely for making final products.

Paste extrusion, on the other hand, can utilize very diverse materials, including cement, clayPlay-Doh, silicone, resin, frosting, UV paste, mashed potatoes, chocolate, etc. Extruding a line of paste onto a build bed is similar to FDM, except that the material is not heated in the nozzle.

Currently, the diameter of paste extrusion can range between 0.0001 mm to 25 cm, enabling the production of cells for organs or print entire buildings from concrete (hardened cement past, HCP) or mud (adobe).

The following manufacturing technology overview is relevant to the use of the proposed 3D infills at structural scales in AM, both for off-site and on-site fabrication. At lower scales, 3D weaving, Selective Laser Sintering (SLS) or Stereolithographic Apparatus (SLA) can also be used to produce the 3D infill patterns.

2.1 Additive manufacturing process

Standard terminology for AM has been outlined in 2015 in the ISO/ASTM 52900-15, Standard Terminology for Additive Manufacturing-General Principles-Terminology. This document [41] was published by the American Society for Testing and Materials (ASTM) International, in collaboration with the International Organization for Standardization (ISO) to define standard terminology for AM. In this document, ISO/ASTM divided AM into seven different processes explained.



Figure 2.1: The entire shelter was assembled by 6-axis robotic arm, which also formatted each individual wooden beam (Masia Can Valldaura, Barcelona, Spain). Photographed by the author in 2018.

2.1.1 Vat Photopolymerization (VP)

A process of selectively curing a liquid light-activated polymer with a laser. An example of this process is stereolithography apparatus (SLA), a technique developed by Charles Hull in the 1980's and commercialized by 3D Systems [12].

2.1.2 Material Jetting (MJ)

A process of selectively depositing drops of material in a layer wise fashion. 3D Systems, Inc. uses this process to print customized dental prosthetic devices such as crowns and copings with high precision using UV curable plastic [12].

2.1.3 Binder Jetting (BJ)

A process of depositing a powdered material layer upon layer and selectively dropping a liquid binding agent onto each layer to bind the powders together. Binder jetting was primarily developed at MIT in a process called 3D printing (3DP) [12].

2.1.4 Material Extrusion (ME)

A process of extruding material through a nozzle and depositing it layer-by-layer onto a substrate. The process was invented by Scott Crump and commercialized by Stratasys as Fused Deposition Modelling (FDM), but it now forms the basis for a very wide variety of inexpensive personal 3D printers [12].

2.1.5 Powder Bed Fusion (PBF)

A process of selectively fusing a powder bed using thermal energy, typically in the form of a laser or electron beam. Selective Laser Sintering (SLS) was developed at the University of Texas at Austin for polymer materials and commercialized by DTM and 3D Systems [12].

2.1.6 Sheet Lamination (SL)

A process of successively shaping and bonding sheets of material to form an object. An example of sheet lamination process is laminated object manufacturing (LOM) developed by Helisys Inc., in which paper sheets were trimmed to size and glued together. Ultrasonic Additive Manufacturing (UAM), commercialized by Solidica Inc., fabricates metal objects using ultrasonic welding [12].

2.1.7 Direct Energy Deposition (DED)

A process of fusing materials with focused thermal energy that melts the material as it is being deposited. An example of this process is laser engineered net shaping (LENS), developed at Sandia National Laboratories, which is particularly useful for repair of damaged metal parts [12].

2.2 Robotic arm systems

The robotic arm printers have the advantage of being more mobile or movable than gantry printers and of being able to print certain prints due to the 6 axis movement that gantry printers would have difficulties with [9].

A robotic arm based 3D printing is more suitable for experienced operators or the robot supplier themselves, and for printing of single elements with high complexity and detail. One of the disadvantages of robot printers is the limited printable area, unless the printer is equipped with a mobile platform, such as wheel or belt chassis.

The users of robotic arm printer is typically limited to structural components, not the entire structures, unless the structure is designed within the reach of the robot, such as the often printed domes with several meters of span.

An example of Kuka six-axis robotic arm system used for additive manufacturing is shown in Figure 4.4 (StrojLab)

In the construction industry, among aggregate-based AM technologies compatible with the robotic arm systems are XtreeE, CyBe and Apis-cor.

Among the polymer-based AM technologies compatible with the robotic arms systems are C-Fab, Digital Construction Platform and FreeFAB Wax.

Metallic Am technology compatible with robotic arm systems is Arup and Permasteel-isa. Detailed description of the above mentioned technology for AM can be found e.g. in the review paper written by Camacho et. al. [8].

2.3 Gantry systems

Gantry printers on the other hand typically have cost and stability advantages, offers the ability to make larger prints and even print entire buildings in one go (as opposed to the more limited prints of robot printers and the robot printers need for printing single elements). Gantry printers also allow for non-continuous printing, which is needed when printing entire buildings, are far more easy to control and does not require highly skilled programmers [9].

Gantry printers are more suitable for more ordinary operators printing a larger variety of prints and for printing much larger structures, up to entire buildings [9].

In the construction industry, among aggregate-based AM technologies compatible with the gantry systems are Pegna, D-Shape, Contour Crafting, Concrete Printing, WinSun, TotalKustom, BetAbram, 3D Concrete Printing (3DCP).

Among the polymer-based AM technologies compatible with the gantry systems are BAAM, Qingdao Unique Products Develop, KamerMaker and Skanska.

Metallic Am technology compatible with gantry systems is MX3D. Detailed description of the above mentioned technology for AM can be found e.g. in the review paper written by Camacho et. al. [8].

2.4 Small robots printing large-scale structures

Although robotics offer great potential towards innovation within the construction industry, their current implementation (robotic arm and gantry systems) applied to the architectural field share a specific limitation. The produced objects are linked to and constrained proportionally to the size of the machine, and the construction process is not scalable.

In order to overcome this limitation, several projects have aimed at developing optionally small, autonomous and swarm intelligence robots, which would utilize drones to extend operational area, climb walls by attaching onto the surface by using a vacuum generator and a suction cup, or attach to the printed structure by clamping it between rollers.

For example, the *Minibuilders* [18] project by the Institute for Advanced Architecture of Catalonia (IAAC) aims to develop a family of small-scale construction robots, all mobile and capable of constructing objects far larger than the robot itself.

An interesting feature of this project is the ability to extrude a second layer over the shell by the vacuum robot and align the extrusion direction with the principal stress direction, i.e. reinforce the shell.

2.5 Cable-driven robots

The required scalability of the construction process could also be reached by relatively simple cable-driven robots. The main advantages of using cable-driven robots for 3D printing in construction are the available six degrees of freedom (DOF), easy installation with simple foundations, low maintenance requirements and very high useful space vs. used space ratio.

The cost of cable-driven systems does not scale with the size of the installation, unlike in the case of gantry or robotic arms systems.

More details can be found e.g. in [16].

Chapter 3

Structural scale applications

Large number of structural scale applications of 3D printing have emerged over the last decade, ranging from indoor sculptures, small shelters to actually used multi-storey buildings. The list of *3D printed house companies* is growing rapidly, each company typically pursues its own *innovative* AM technology, as can be seen in the previous section on different 3D printing systems. A detailed review can be found e.g. in [8].

For a brief introduction (source: google.com and www.3dnatives.com), the currently most recognized systems are listed:

- Apis Cor has developed a 3D printer capable of building a house in 24 hours. The machine is 4.5 metres long, 1.5 metres high and wide, and can be easily transported by crane. It is a polar 3D printer that extrudes concrete on a 132m² printing surface, rather than a printer installed on a gantry and rails.
- BatiPrint has developed a new 3D printing technology for house construction. This allowed them to 3D print the first social housing in Nantes. They have developed a 4 metre long robot that deposits 3 layers of materials at once. This material includes two layers of expansive foam, and one third concrete. In addition, the robot is portable, and can be operated directly on-site. The printer is capable of building walls 7 metres high.
- WASP has developed a concrete 3D printer which is the largest currently on the market. The 12 metre tall and 7 metre wide 3D printer has adjustable arms up to 6 metres long. The printer, called the BigDelta, aims to respond to the housing crisis by building cheaper homes, especially for developing countries. The long-term goal of the project is for the BigDelta to be able to extrude straw and earth.
- KamerMaker (Ultimaker & DUS Architects) has started making 3D printed houses in 2012. They developed the FDM 3D printer with very large printing dimensions: 2 x 2 x 3.5 m. The aim of this project is to help construct houses from recycled materials sourced locally. So far, DUS Architects have completed a few projects such as their project of the Casad del Canal, and a cabin in Amsterdam.
- WinSun has created the first 3D printed house. They use a machine based on FDM technology and uses the same layer-by-layer process with cement, sand, and fibres. They develop walls for houses in their factory before moving them on-site, with their 32 x 10 x 6.6 m size 3D printer. In addition to their first project in Shanghai, they developed the first 3D printed offices in Dubai back in 2016, and have collaborated with Elon Musk to develop Hyperloop tunnels. They have also recently 3D printed a number of concrete bus stops in China.

- Cazza Construction has been chosen to develop the first 3D printed skyscraper in Dubai. At the end of 2017, Cazza presented their first 3D printing robot, the Cazza X1. This machine can lift 90kg, and has a maximum range of 3.9-4.7 metres depending on its extension.
- Constructions-3D aims to build customisable homes from recyclable materials that are sourced locally. They use a *concrete crane* based on FDM.
- Contour Crafting use a *quick-setting, concrete-like material* which is deposited layer-by-layer until the build is finished. Technical parts like plumbing and wires can be added as the layers are being built.
- CyBe Construction has a mission to revolutionise concrete 3D printing with applications to home construction. They produce 2 concrete 3D printers, the CyBe RC 3Dp, The CyBe R 3Dp, as well as their MORTAR material. These large, industrial 3D printers require two operators to oversee production, but the printer can print large structures in just 20 minutes due to its fast 200mm/s printing speed.
- D-Shape uses binder jetting technologies with a material which mixes sand, seawater, and a binding agent of magnesium and can make large structures out of this *stone-like* material. The current version of the D-Shape fits roughly inside a 6m x 6m frame and the printhead has 300 nozzles spaced 20mm apart to print the stone solution.
- XTreeE aims to pioneer industrial scale additive manufacturing with concrete, and build houses and other structures. They are known for creating a variety of *interesting pieces* with complex architectures, such as a 4 metre tall pillar.

In their recent book [36], Rael and San Fratello published innovative recipes for 3D printing, including a number of DIY recipes for liquid binders and powders. Although 3D printing in general can utilize almost any known material, including salt, sawdust, coffee, rubber, bioplastics, cement, sand or clay, the following discussion will be limited to selected aspects relating to more traditional cementitious composites, adobe and polymers.

3.1 Concrete

Additive manufacturing and digital fabrication bring new horizons to concrete and cement-based material construction. The possibility to build concrete structures without formwork is a major advantage in terms of production rate, architectural freedom and cost reduction, while the formwork represents 35–60 % of the overall costs of concrete structures [25].

Required parameters of concrete used for large-scale 3D printers is flow-ability and fast strength gain. For this reason, researchers focus on understanding and controlling the rheology of the printed paste and investigate means of stiffening control, such as in the ongoing project *Smart Casting of Concrete Structures by means of active rheology and stiffening control* of the Magnel Laboratory for Concrete Research, embedded within the Department of Structural Engineering at the Faculty of Engineering and Architecture of Ghent University. The goal of this project is the active control of concrete rheology during casting, and the active triggering of early stiffening of the concrete as soon as it is put in place. The ground-breaking idea to achieve this goal, is to develop concrete with actively controllable rheology by adding admixtures responsive to externally activated electromagnetic frequencies.

Given the fact, that the standard reinforcement bars can only be inserted manually during the print, or can be inserted by another robotic arm, the concrete can either be plain (for small structures) or reinforced by steel or polymer fibres.

Despite the ongoing effort and a number of available AM technologies for concrete (see chapter Construction 4.0), the technologies for scaling-up desktop 3D printer to a size of a building site are not sufficiently developed for industrial application, and the above mentioned list of systems still represents project in more of experimental than production phase.

3.2 Adobe

The story of architecture for thousands of years has been the story of mud. With the popularization and rapid development of 3D printing, the technology community increasingly find interest in clay, earth, and other locally sourced, renewable materials that possess intrinsic and enduring qualities: humidity regulation, structural stability, natural cooling, etc. Available techniques for 3D printing clay are powder-based (jet-binding technology) or paste-extrusion printers that use moistened clay. Scale of printed objects range from vases and bricks to large structures, such those fabricated by the *World's Advanced Saving Project* (WASP, www.3dwasp.com). In this project clay is used to extrude structural components with the goal to construct a sustainable village composed of 3D printed mud houses. The mud can be sourced locally with little infrastructure and no industrial or expensive materials. The mud is strengthened by straw and baked solely by the sun, forming an adobe.

Emerging Objects introduced the *Cool Brick* in 2015 (www.emergingobjects.com), which are modular and interlocking, and can be stacked together to make a screen. The 3D lattice creates a strong bond when set in mortar. The shape of the brick also creates a shaded surface on the wall to keep a large percentage of the wall's surface cool and protected from the sun to improve the wall's performance.

In a similar initiative of IAAC, *Terraperforma* focused on large-scale 3D printing with a traditional material, unfired clay, and climatic performative design (<https://iaac.net>).

The clear limitation of adobe is that construction location has to be limited to dry and hot climates, if to be used without protection.

3.3 Polymers

Although polymer based 3D printing rarely scales up to buildings and infrastructure, several buildings have been fabricated recently, including the *World's Largest 3D-Printed Polymer Building* designed by SOM and Oak Ridge National Laboratory, who optimized the structure's form to reduce the amount of material used and to express three-dimensional printing's ability to deploy complex, organic geometries. The dimensions of the printed structure are 11.6 x 3.7 x 3.7 meters.

In another application, DUS Architects have combined 3D-printed bioplastic with a tensile fabric structure to create a sculptural facade for the Mobile Europe Building, the elements are recyclable and can be created up to a size of 5 x 2 x 2 meters. This group is also included in the *3D Print Canal House*, a three-year 'Research & Design by Doing' project, which uses the Kámer Maker AM system.

As large quantities of recycled materials are currently available, often for free, there is clearly a demand for their utilization also in the AM process. Within the cooperation with

the Department of Reverse Engineering and Additive Technologies, Institute of Machine and Industrial Design, at Faculty of Mechanical Engineering, extrusion of recycled PET binder with recycled glass aggregates is developed, for which serves a 6-axis robotic Kuka arm (fig. 4.4) equipped with in-house developed extruder. Author of this thesis is involved by designing and managing experimental short term and sustained load tests as well as environmental tests.

FDM-based 3D printers are presently the most popular consumer-level 3D printers for printing polymer composites. Among other extrusion-based techniques, FDM is a material-melting technique which uses a spool of thermoplastic filament such as PC, ABS and PLA with varying diameters to be melted and extruded through a heated nozzle.

A general disadvantage of FDM is the filament itself must be fabricated with a high quality because the feeding (tension and compression) and melting (heating) action of FDM will test its mechanical and thermal stability.

For larger printers, however, the filament can be replaced with granular form of the material, which reduces the above mentioned limitation.

Chapter 4

Collaborative research

The activities presented in this thesis have been conducted as a collaborative research between several university laboratories.

The AdMaS (Advanced Materials, Structures and Technologies) science centre (fig. 4.1) and comprehensive civil engineering research institution is part of the Faculty of Civil Engineering at Brno University of Technology. It focuses on research and development in the area of advanced construction materials, structures and technologies, and their real-world application in not only the construction industry, but also transportation systems and the infrastructures of cities and municipalities. The author of this thesis runs a 3D printing laboratory (fig. 4.2) in this research center, where the tested specimens have been produced, and which annually introduces the research topics to the public within the Night of Science event. In particular, the large scale industrial FDM printer Builder 2000 (fig. 9.1) and desktop FDM printer Prusa i3 MK2 (fig. 9.2) is utilized, together with industrial optical 3D scanner from Rangevision, which is used to compare the printouts with the digital models.

The structural testing of the specimens has been carried out at the structural testing laboratory within the Department of Civil Engineering and Natural Hazards, Institute of Structural Engineering (IKI), University of Natural Resources and Life Sciences, Vienna. Here, a hydraulic testing machine with a Digital Image Correlation System has been used for the compression tests, and the anisotropic behavior associated with a layer-based production processes was evaluated by tensile tests on standard “dog bone” (DB) specimens.

In order to upscale to architectural scales, a cooperation with the Department of Reverse Engineering and Additive Technologies, Institute of Machine and Industrial Design, at Faculty of Mechanical Engineering has been established. Currently, gantry type printer for concrete and mortars is developed, enabling multi-meter build volumes and high degree of detail. Additionally, extrusion of recycled PET binder with recycled glass aggregates is also developed, for which serves a 6-axis robotic Kuka arm (fig. 4.4) equipped with in-house developed extruder. Author of this thesis is involved by designing and managing experimental short term and sustained load tests as well as environmental tests.

Technology Agency of the Czech Republic granted to author of this thesis an applied research project, the aim of which is to develop a unique vacuum coating system for rapid prototyping (VPAT). This project is based on cooperation with ČEGAN s.r.o., where vacuum coating is applied to injection-moulded parts. Successful application of the vacuum coating technology to 3D printed objects will strengthen the position of both applicants in Industry 4.0 and increase their competitiveness. In regard to the application of highly porous structures and known materials for 3D printing, surface finish is an important durability aspect, where the traditional surface finishing options are not longer effective due to the presence of hardly accessible voids. Gravity effects are known to cause problems when heat-treating or soaking the specimens.

Recently, a collaboration with Magnel Laboratory for Concrete Research has been established on the topic of mechanics of ageing of printed concrete and recycled polymer structures and related environmental aspects. This laboratory is embedded within the Department of Structural Engineering at the Faculty of Engineering and Architecture of Ghent University.



Figure 4.1: Science centre and comprehensive civil engineering research institution AdMaS (Advanced Materials, Structures and Technologies). Retrieved from www.admas.cz



Figure 4.2: Every year the 3D printing lab at AdMaS participates at a public event for public (Night of Science). Photographed by the author in 2018.



Figure 4.3: The structural testing laboratory within the Department of Civil Engineering and Natural Hazards, Institute of Structural Engineering (IKI), University of Natural Resources and Life Sciences, Vienna. Photographed by the author in 2018.



Figure 4.4: Kuka six-axis robot and additive manufacturing at StrojLab, which is part the Fab Lab global network. Retrieved from www.strojlab.cz

Part II

Generative design

Chapter 5

Motivation by topology optimization

With the development of technology and computers science, new possibilities for structural design occur, and engineers are not limited any more to hand calculations and simplified approaches. The design approach termed topology optimization can be used to determine the optimal topology of a structure in order to obtain the desired functional performance. Improving structural performance, it has been widely used in most engineering fields, for example, automotive and aerospace industries extensively use topology optimization in order to reduce weight and increase stiffness for decades.

The requirement of sustainable structural design implies applying optimization techniques also for reinforced concrete design, as cement production is responsible for roughly 5% of man-made carbon dioxide emissions annually [28]. In fact, 900 kg of CO₂ are emitted for every 1000 kg of cement produced [27]. This motivates the search for design methodologies that facilitate weight reduction of concrete structures while maintaining the required load carrying capacity.

The growing interest within the architectural community in topology optimization as a means of generating aesthetic and efficient structural forms is another motivating factor (e.g. see [5], [42]). Until recently, standard topology optimization procedures aimed at minimizing compliance of a linear-elastic structure were utilized for this purpose, overlooking the true behavior of the construction material, especially in the case of concrete [5]).

A number of studies attempting to incorporate more realistic modelling with respect to reinforced concrete exist. For example, different stiffness can be considered for concrete and steel, the true behaviour of concrete as a brittle strain-softening material can be considered, as well as the realistic volume of steel, to name the few. Advanced numerical methods are available and new trends are regularly discussed on scientific conferences worldwide [15], and since the scope of this thesis is spatial materials for additive manufacturing, the aspects of realistic material modelling will not be further detailed in this chapter. The following discussion will serve as a motivation and application domain for the presented spatial materials.

Although the classical theories of continuum and discrete mechanics can approximate the stress field reasonably well for any given structural member, the final design of such member rarely reflects the principles of optimized inner forces given a certain material, as many fabrication constraints have to be taken into account. Examples are the cost of the formwork or concrete casting and consolidation [22].

If such constraints are removed by the 3D printing process, existing numerical methods can be used to optimize the material utilization within a given structure with respect to given loading, boundary conditions and other performance oriented goals (e.g. acoustic or thermal). Not surprisingly, such optimization results in lightweight, non-prismatic and streamlined structures, often resembling shapes which can be found in nature at various scales – from branching structures like trees down to biological membranes. Please note that the term

bio-inspired or organic is often used by architects and designers who apply or get inspired by the principles from nature, while, the same design principles can emerge from a simple numerical optimization based on straight forward mechanical principles. Through this paper the term organic refers to the outer shape of a structure, directly obtained by numerical topology optimization. The term bio-inspired, furthermore, refers to the infill patterns, the shapes of which do not originate from a topology optimization process but were described by mathematicians who supposedly were inspired by nature some 140 years ago.

5.1 Transition to branching structures

Development of technology gives us more options how to reliably design non-prismatic columns. One reason is, that software packages used for design and assessment, can be, if properly used, much more precise than simplified approaches suitable for hand calculation. Another aspect is construction feasibility. Contemporary expansion of additive manufacturing, commonly known as 3D printing or fused deposition modelling (FDM), has caused, that this technology is finding its way even to traditional areas such as civil engineering.

Currently, this method is still under development and a large amount of research has to be done before it will be ready to be massively used for construction. However, for the places, which are remote from classical resources, the additive manufacturing may eventually be the best option. Building outposts at Antarctica or on the Moon or Mars from the local material may be significantly more efficient than carrying that material from the Earth [6]. This technology can also be attractive for prefabricated construction, since large-scale printers with other necessary equipment can be placed inside a factory itself [23].

To get an insight how these organic shapes should look like, an inspiration can be taken from nature where plenty of structures are already optimized by millions of years of evolution. A good example is a tree – seemingly very light structure capable of withstanding even strong winds. However, this shape cannot be directly applied to structural columns since the tree is meant to carry only its own weight not much greater dynamic loads from above. Another example is long bones like the femur, capable of transmitting much greater loads than their own weight. This bone is very slender and almost cylindrical in its cross-section, with sponge-like inner structure, mostly visible around its ends. Research showed, that this shape is adapted to carry maximal load with minimal material requirements [7].

One way how to design such organic shapes is by using topology optimization. It is a method that optimizes material for given load and boundary condition, which usually yields in non-prismatic organic-like shape. An experiment was performed in structural software IDEA StatiCa [3]. A rectangle wall with dimensions 5.0 x 3.0 x 0.2 m was loaded with a uniformly distributed line load on its top edge. The wall was then supported by three-point supports with bearing plates 0.2 m wide (Figure 5.1). A topological optimization was performed with a target volume of 20 % of the original structure. The result showed rather complex branching structure, that would be optimal to transmit the load to the supports (Figure 5.2).

This example demonstrates the possible transfer from current rectangular systems with prismatic members to more complex organic structures. With the development of additive manufacturing engineers can design complex organic shapes with a non-solid inner structure (Figure 5.3) that can also be optimized to more efficient shapes for any given load case. Static vertical loads require different column shapes than dynamical loading from various directions,

which yields a multi-scale problem, for which the solution depends on scale considered. The final optimal structure will, therefore, be different for each loading case. During the production process (3D printing), the material can also be deposited along the lines of principle stress instead of horizontal layers in order to maximize structural performance [24].

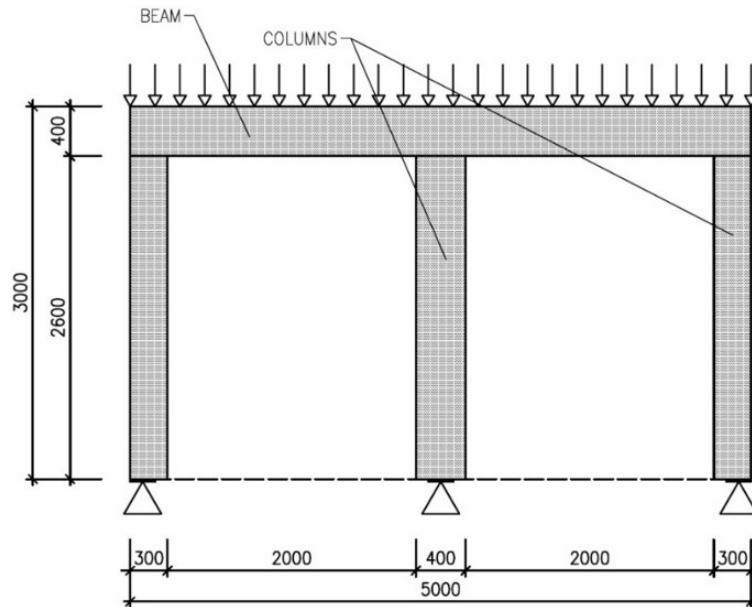


Figure 5.1: Example of classical design approach. Source: co-authored [22]

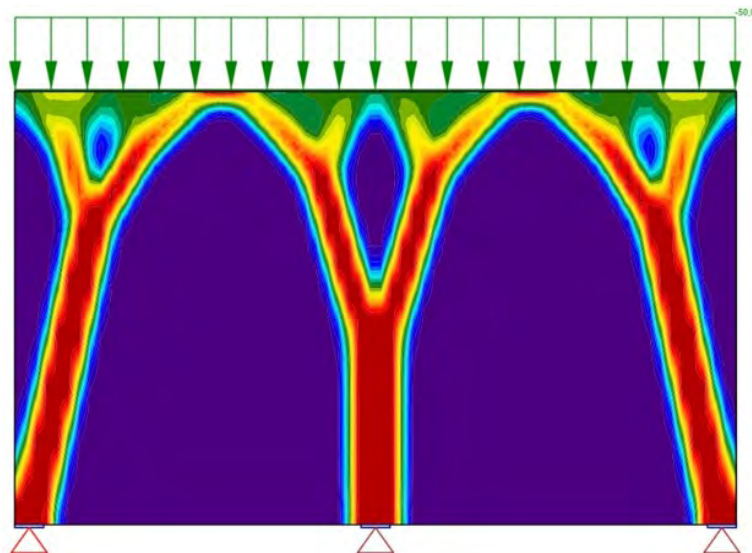


Figure 5.2: Topological optimization in IDEA StatiCa (Red parts are more utilized, blue parts are less utilized). Source: co-authored [22]

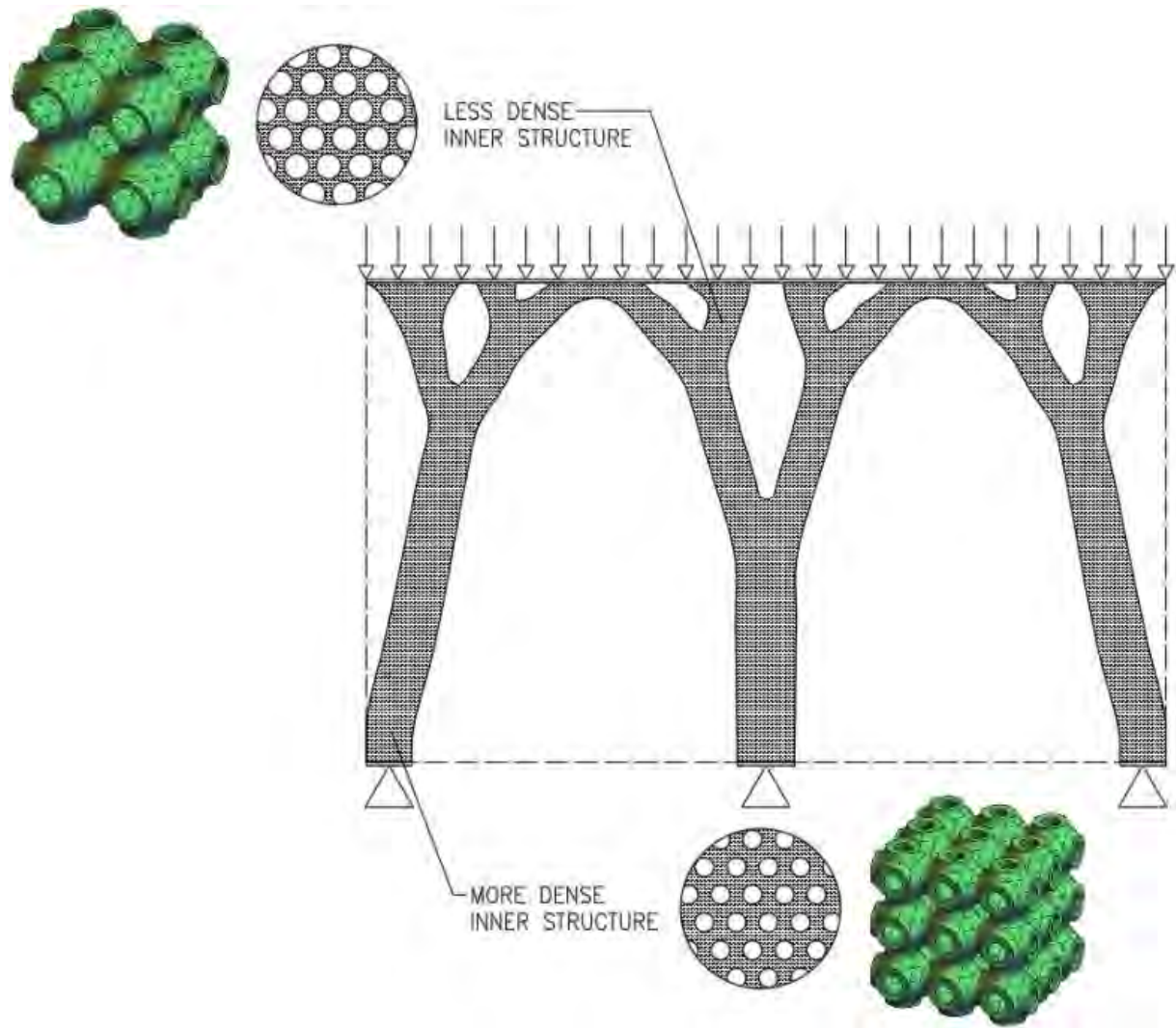


Figure 5.3: Optimised organic frame with variable density governed by bio-inspired 3D infill). Source: co-authored [22]

5.2 Generated organic structures

Traditional design approaches do not make the most of new manufacturing methods, like additive manufacturing, which remove design constraints and at the same time bring new possibilities. The optimal shape of a structure or component is often organic and counter-intuitive, so designing it requires a different approach. The presented examples have been generated using the Topology optimization tool in ANSYS Mechanical [2]. The classical workflow is presented in Figure 5.4, where the initially solid element is discretized into finite elements and consequently reduced by removing the least stressed elements until a mass fraction goal is met (Figure 5.5).

A transition from classical column to (organic) branching structures is shown in Figure 5.6, for which a linear Finite Element Model (FEM) model was repetitively run while removing the least-utilized material with respect to stress. Note that this approach is sensitive to

discretization, i.e. to the size of elements, and according to the fractal principle, with increasingly small elements and decreasing mass fraction to be retained, self-similar branching can be observed on the perimeter of the initially defined solid body.

This example can be interpreted as roof support, and serves as a motivation for the subsequent analysis of various infill options.

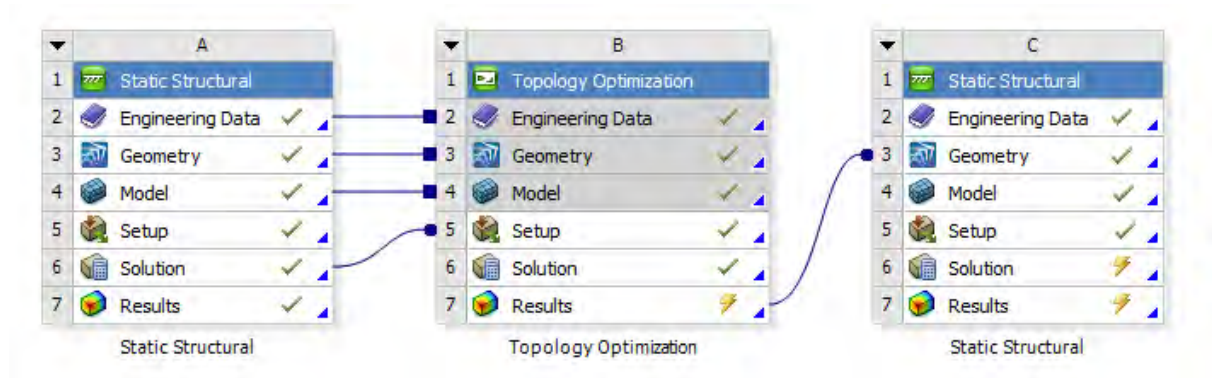


Figure 5.4: Classical topology optimization work-flow in Ansys Workbench 19.1. Figure by author.



Figure 5.5: Classical topology optimization principle: initially defined solid body with boundary conditions (left) and the retained 15% mass after iterative removal of least stressed elements. Figure by author.

Another example of emergent organic structure is the simply supported beam element with uniformly distributed load at the bottom face (Figure 5.7). Here, similarly to the column



Figure 5.6: Printouts of topology optimization results and fractal principle: element size governs the overall shape. Photographed by author in 2018.

example, with reducing mass ratio to be retained, self-similar branching emerges, following the same principle as many natural systems, such as trees.

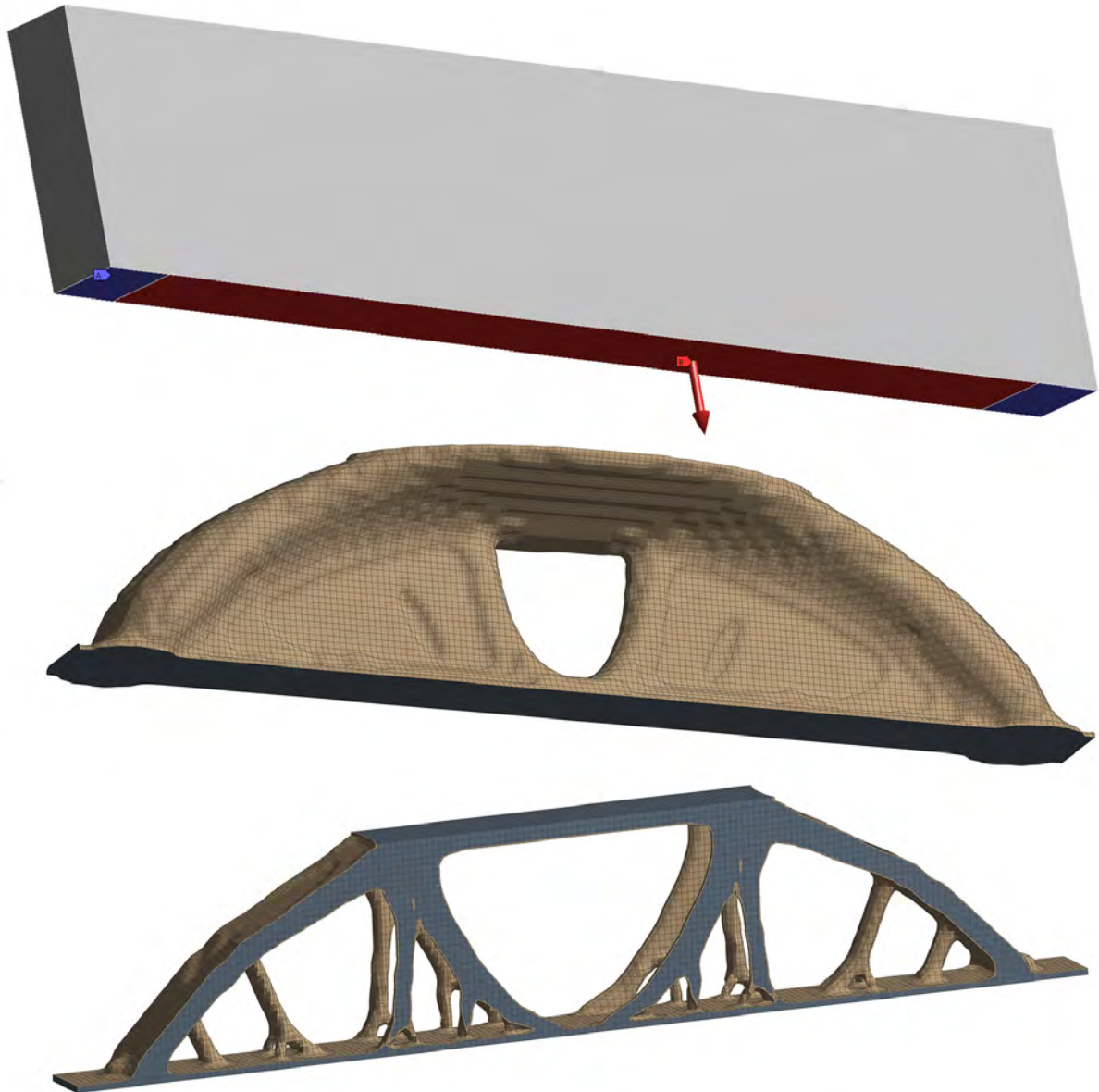


Figure 5.7: Classical topology optimization beam example with two levels of retained mass (left 30%, right 15%) and uniformly distributed load (red) at the bottom face of the supported (blue) beam. Figure by author.

Chapter 6

Multi-scale optimization

In 3D printing infill densities close to 100% are rarely used, as opposed to traditional casting process. Figures 6.1 and 6.2 shows a detail of this branching structure (15% infill density), which illustrates how classical 2D infill patterns (such as honeycomb) cannot be aligned with the principal stress direction, while the gyroid 3D infill forms a porous infill with constant curvature, no planes of symmetry and no embedded straight lines. Such infill properties without preferential direction are useful when complex 3D geometries under general stress states are considered.

Possible infill parameters and the associated choices with respect to multi-scale optimization are depicted in Figure 6.3, where several functional forms (or periodic implicit formulation), macro-scale characterization (length scale), shell (wall) thickness and random/irregular components are shown for illustration purposes.

The manipulation of the above mentioned infill parameters potentially offers benefits in terms of tuned thermal, acoustic, static or dynamic properties, and can be further used to locally map the infill density to actual stress fields, i.e. to manipulate infill wall thickness or infill feature size in order to achieve uniformly distributed stress (Figure 6.4). As this mapping can be fully automated and integrated in the computational design and digital fabrication process at no additional cost, there is no reason not to consider it.



Figure 6.1: Detail of a branching structure and 3D infill (gyroid). Figure by author.



Figure 6.2: Detail of a branching structure and 2D infill (hexagonal). Figure by author.

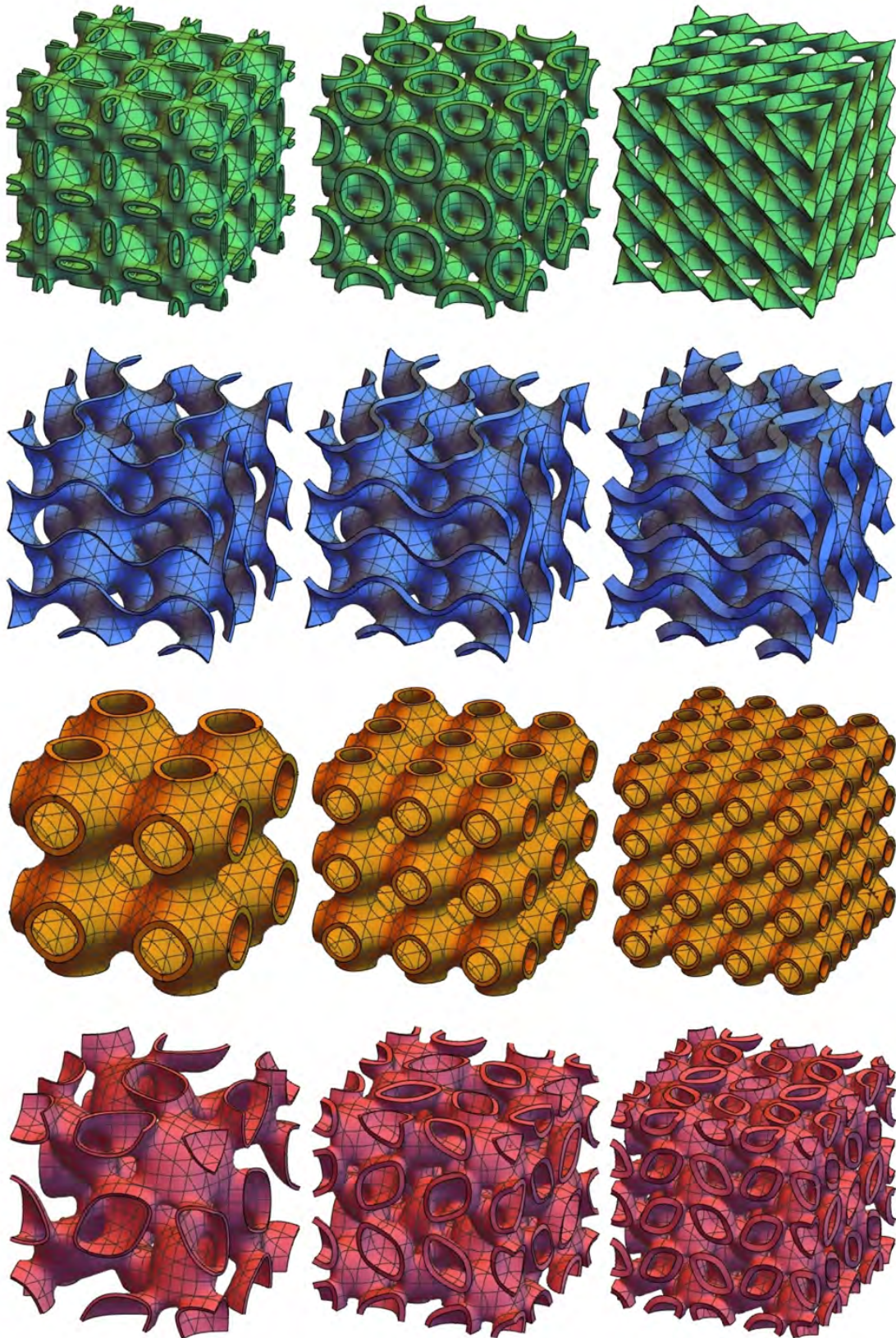


Figure 6.3: Choices associated with 3D infills and multi-scale optimization: periodic implicit formulation (green), macro-scale characterization (orange), shell thickness (blue) and random/irregular components (red). Figure by author.

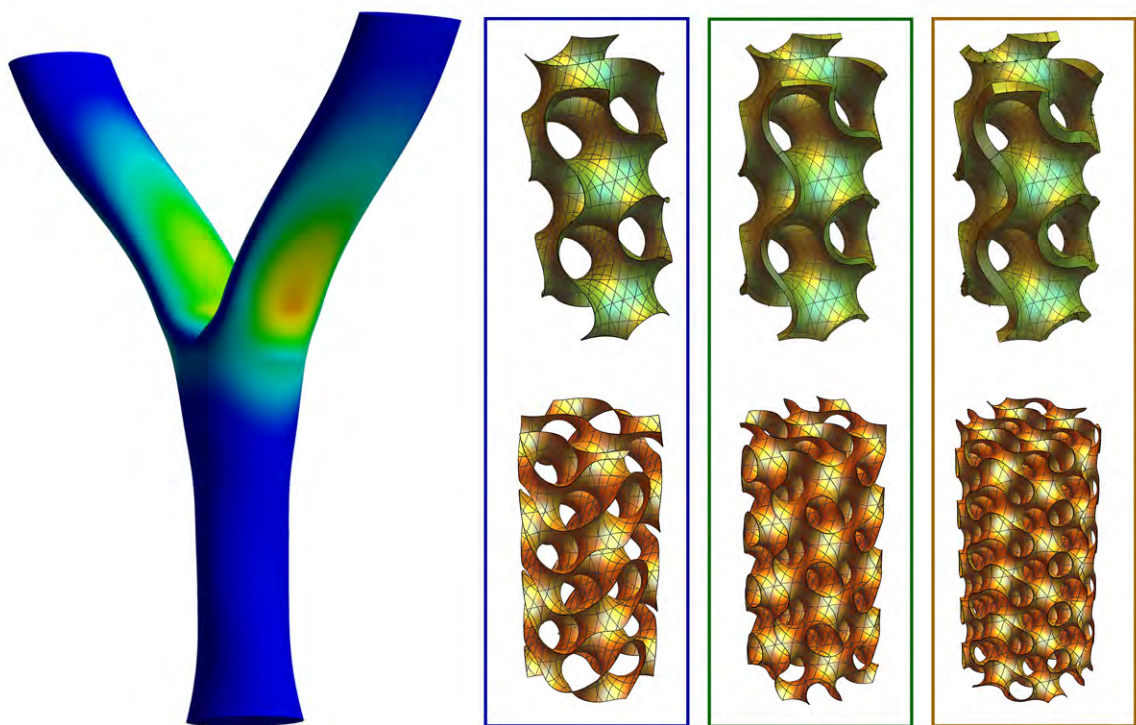


Figure 6.4: Principle of mapping local stress levels to infill thickness or scale. Figure by author.

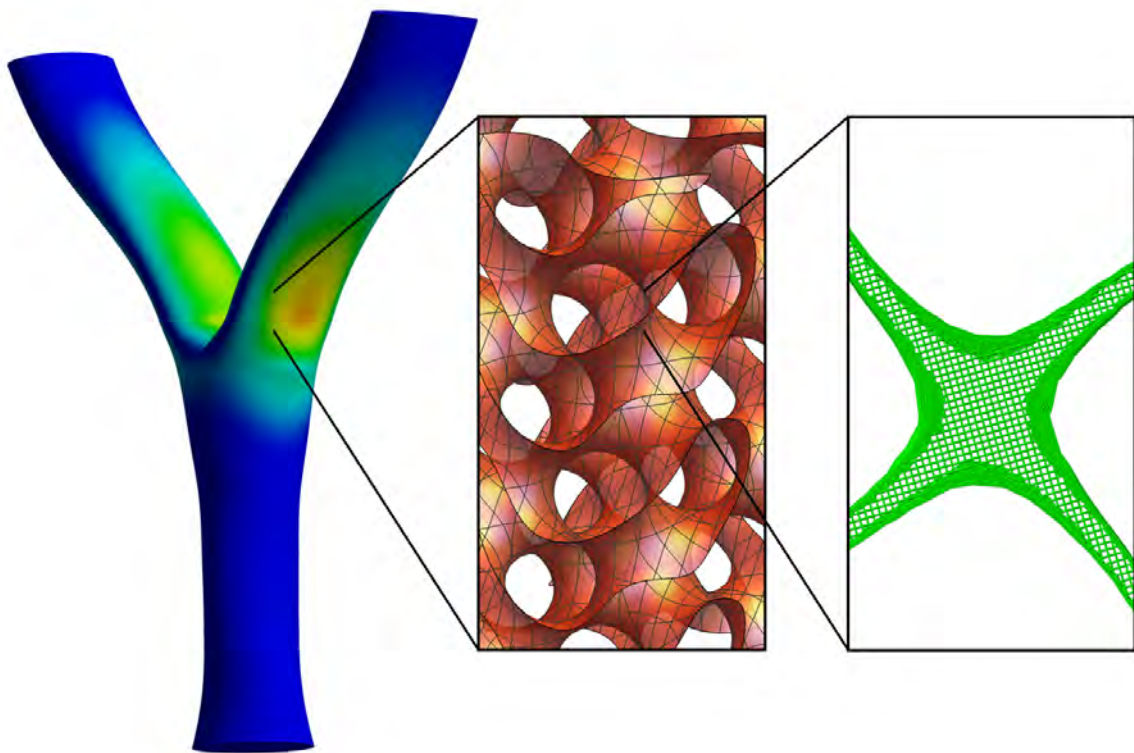


Figure 6.5: Principle of multi-scale optimization: from outer shape (left), infill type (center) to infill wall composition (extruder travel moves and density). Figure by author.

Chapter 7

Periodic minimal surfaces

There is a great number of minimal periodic surfaces that can be used as shapes for inner structure of columns and other structural members. A research by NASA [38] has already been done in 1970 to show the potential of such shaped materials for the space industry. A research on selected six of these minimal periodic surfaces was performed for the sake of this paper, to get an insight into their basic properties. Points in a given cube matrix with a base size of 4π were generated using the parametric equations shown in 7.1 in order to obtain a representative volume element (RVE).

The tolerance parameter t used in the equations correlates with the thickness of the surfaces walls - the higher t , the thicker the walls and the denser the RVE.

Visualizations of the selected point clouds are shown in 7.1.

7.2 shows input parameters and 7.3 output parameters of the six minimal periodic surfaces. With relative volumes spanning from 14 % to 29 % of the solid cube, the resulting RVE mass is down to 330 kg/m^3 to 680 kg/m^3 (compared to 2360 kg/m^3 for regular concrete, $1400\text{-}1800 \text{ kg/m}^3$ for lightweight concrete or $650\text{-}700 \text{ kg/m}^3$ for ultra-lightweight concrete). A significant portion of the load carried by concrete structural members stems from the dead weight of the structure itself. Therefore, even small changes in the performance ratio (strength/volume mass) can lead to more efficient and cheaper structures. Also, the structure can be tuned for the static and dynamic response, have custom failure modes or tailored acoustic and thermal properties. The concrete formed into the shape of periodic surfaces with relatively thin walls can also have different shrinkage and creep behaviour than in the solid form.

Research has to be done to find the optimal geometrical configuration of inner structures for different loading patterns, materials or structural parts. Even small changes in the parametric formulation will result in substantially different structure and, thus, different RVEs with different optimum parameters. An experiment on 3D printed minimal periodic cubes was recently performed e.g. by MIT [35]. It showed, among others, that the resistance and deformation capacity may be strongly influenced by the shell thickness only. In terms of

Table 7.1: Equations of surveyed minimal periodic surfaces.

Name	Equation
Gyroid	$(0 - t) < \sin(x)\cos(y) + \sin(y)\cos(z) + \sin(z)\cos(x) > (0 + t)$
Gyroid Squared*	$(1 - t) < (\sin(x)\cos(y))^2 + (\sin(y)\cos(z))^2 + (\sin(z)\cos(x))^2 > (1 + t)$
Gyroid Tripled*	$(0 - t) < (\sin(x)\cos(y))^3 + (\sin(y)\cos(z))^3 + (\sin(z)\cos(x))^3 > (0 + t)$
Schwarz P	$(0 - t) < \cos(x) + \cos(y) + \cos(z) > (0 + t)$
Schwarz D	$(0 - t) < \sin(x)\sin(y)\sin(z) + \sin(x)\cos(y)\cos(z) + \cos(x)\sin(y)\cos(z) + \cos(x)\cos(y)\sin(z) > (0 + t)$
Neovius	$(0 - t) < 3(\cos(x) + \cos(y) + \cos(z)) + 4 \cos(x)\cos(y)\cos(z) > (0 + t)$

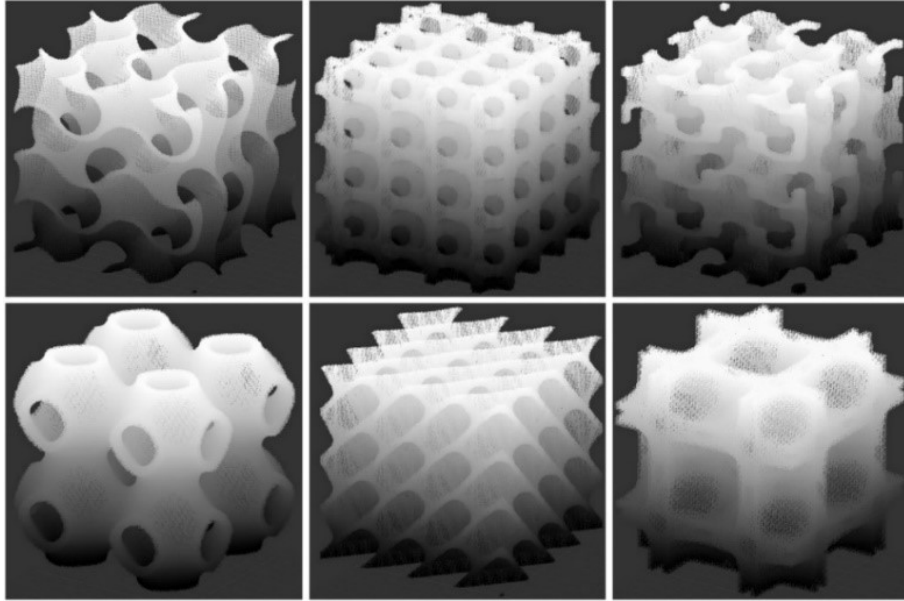


Figure 7.1: Generated shapes (from upper left): (a) Gyroid, (b) Gyroid Squared R, (c) Gyroid Tripled, (d) Schwarz P, (e) Schwarz D, (f) Neovius. Source: co-authored [22]

Table 7.2: Input parameters of surveyed minimal periodic surfaces.

Name	Base size	Tolerance t	Step
Gyroid	4π	0.20	0.10
Gyroid Squared	4π	0.10	0.10
Gyroid Tripled	4π	0.20	0.10
Schwarz P	4π	0.30	0.10
Gyroid	4π	0.25	0.10
Gyroid	4π	0.80	0.10

inner structure optimization, there are five aspects to consider in general. These are the periodic implicit formulation, its period length, shell thickness, shell density, and systematic/random spatial variation [31] of the aforementioned. By considering different optimization goals (structural, thermal, acoustic, durability, costs, aesthetic) in combination with the five optimization aspects mentioned above, the dimensionality of the problem may clearly become prohibitive from optimization point of view. As seen often in nature, the fractal principle may be also applied to the shell thickness and density, where solid infill is not preferable and standard infill patterns (rectangular, triangular, honeycomb, etc.) should be applied to optimize production (3D printing) speed, among others.

Author's contribution to durability and robustness aspects can be found e.g. in [45] or [32]. Author's contribution to lifecycle robustness and design can be found e.g. in [34] or [46].

When analysing organic structural members or structures, we need to keep in mind that it is a multi-scale problem and the structure can be analysed on three levels. On a structural level, the overall shape of the structural member is designed using some optimization method such as topology optimization. The inner spatial structure is analysed on a macro level as the

Table 7.3: Calculated parameters of surveyed minimal periodic surfaces.

Name	Locations	Points	Density
Gyroid	1 953 125	252 421	12.92 %
Gyroid Squared	1 953 125	252 421	29.11 %
Gyroid Tripled	1 953 125	252 421	22.60 %
Schwarz P	1 953 125	252 421	17.18 %
Gyroid	1 953 125	252 421	20.56 %
Gyroid	1 953 125	252 421	34.77 %

cross-section does not need to be solid using additive manufacturing. There are shapes known as minimal periodic surfaces that can be an option for the microstructure. Great advantage of these surfaces is, that they do not contain any sharp edges causing peaks in stress flow. Finally, we also need to consider the material level where the performance depends on the parameters of the used material and technology.

7.1 RVE characterization

A way has to be found to safely and efficiently design and analyse branching structural members consisting of non-solid spatial materials. Since the structure of the minimal periodic surface is rather fine, compared to the size of the whole structural member, it would be inefficient to model whole structures as precisely. Provided the parameters of the periodic surfaces are known, one possible way is to homogenize the structure [29]. Parameters such as compressive strength or volume mass have to be either measured or calculated on a small scale and transferred to standard finite or discrete element formulations on the macro-scale. When characterizing structural concrete, or any other heterogeneous random material, for numerical assessment, the statistical and spatially variable properties of aggregates, pores or fibre reinforcement [47] may be computationally intensive. The proposed periodic implicit formulation, on the other hand, may represent possible advantage, as the RVE can be directly linked to selected period (scale), without the need for costly analysis. As for the nature and complexity of the resulting structures, a possible way how to model these in small scale is to use specialized computational software like MARS [10]. Among others, this software implements the recently introduced Lattice Discrete Particle Model (LDPM), which uses a discrete framework (particles) to model displacement field [10, 33]. Contrary to the traditional Finite Element Method (FEM), where the continuous framework is used, LDPM is ideally suited for modelling post-limit fracturing and the shattering of material (see Figures 7.2, 7.3 and 7.4). Once the properties on the microscale are defined, whole structural members can be designed. Using concrete for 3D printed civil structures would be the first option since it can be formed into various shapes. It is the periodic geometrical form that may be advantageous over the solid one.

To get initial insight into the behaviour resulting from a periodic inner structure, a compression test on a cylindrical gyroid sample with diameter of 150 mm printed from PLA was performed. The parametric equation of gyroid can be found in Table 1. Young's modulus of typical PLA spans between 3.5 to 6.5 GPa [11] and compressive strength between 18 to 90 GPa [44] compared to Young's modulus between 32 to 44 GPa and strength between 30 to 90 MPa for typical concrete. Sample before compression test is shown in Figure 5. The

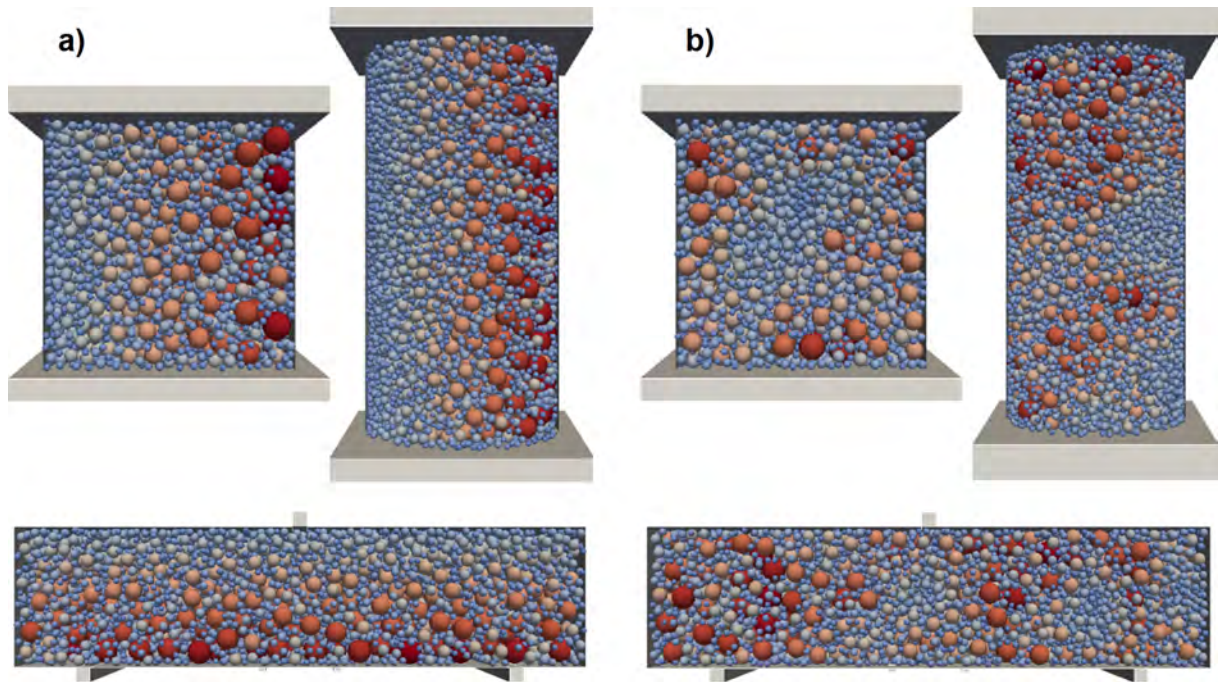


Figure 7.2: LDPM models of classical concrete experiments and particle placement governed by gradient-based fields (a) and random fields (b). Figure by author.

load-displacement diagram shown in Figure 6 reveals a steady linear load increase up to 85 % the of peak strength. After the maximum load capacity was reached at the load of 44 kN, the sample showed a small drop in resistance followed by large deformation capacity before it was completely crashed. Before the end of the experiment, resistance of the sample increased again. This was caused by the fact, that crushed shells locked into each other, filling the previously empty space and, therefore, supporting the whole structure.

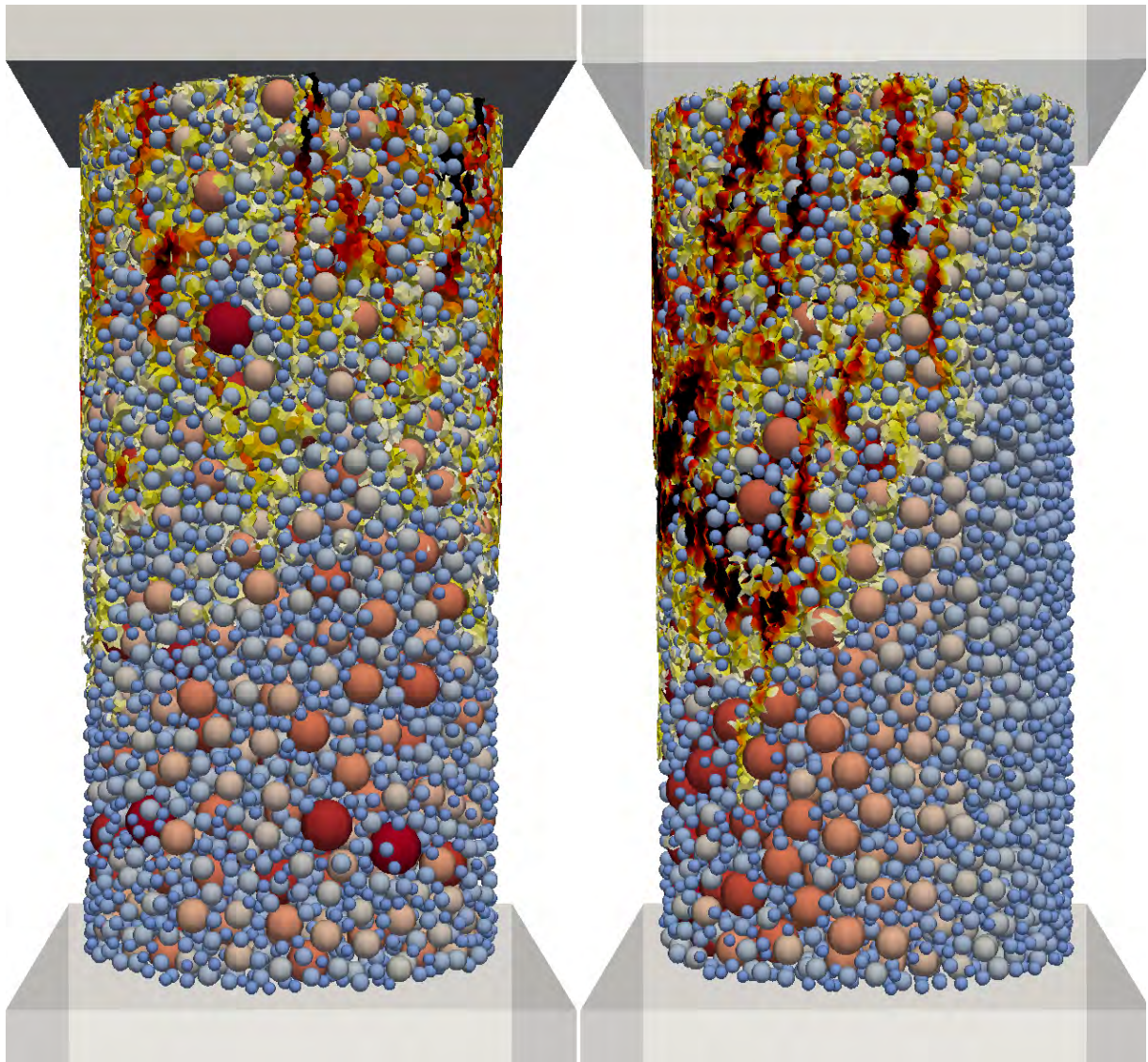


Figure 7.3: Example of qualitatively different failure modes of LDPM models resulting from microstructural differences and governing random fields. Figure by author.

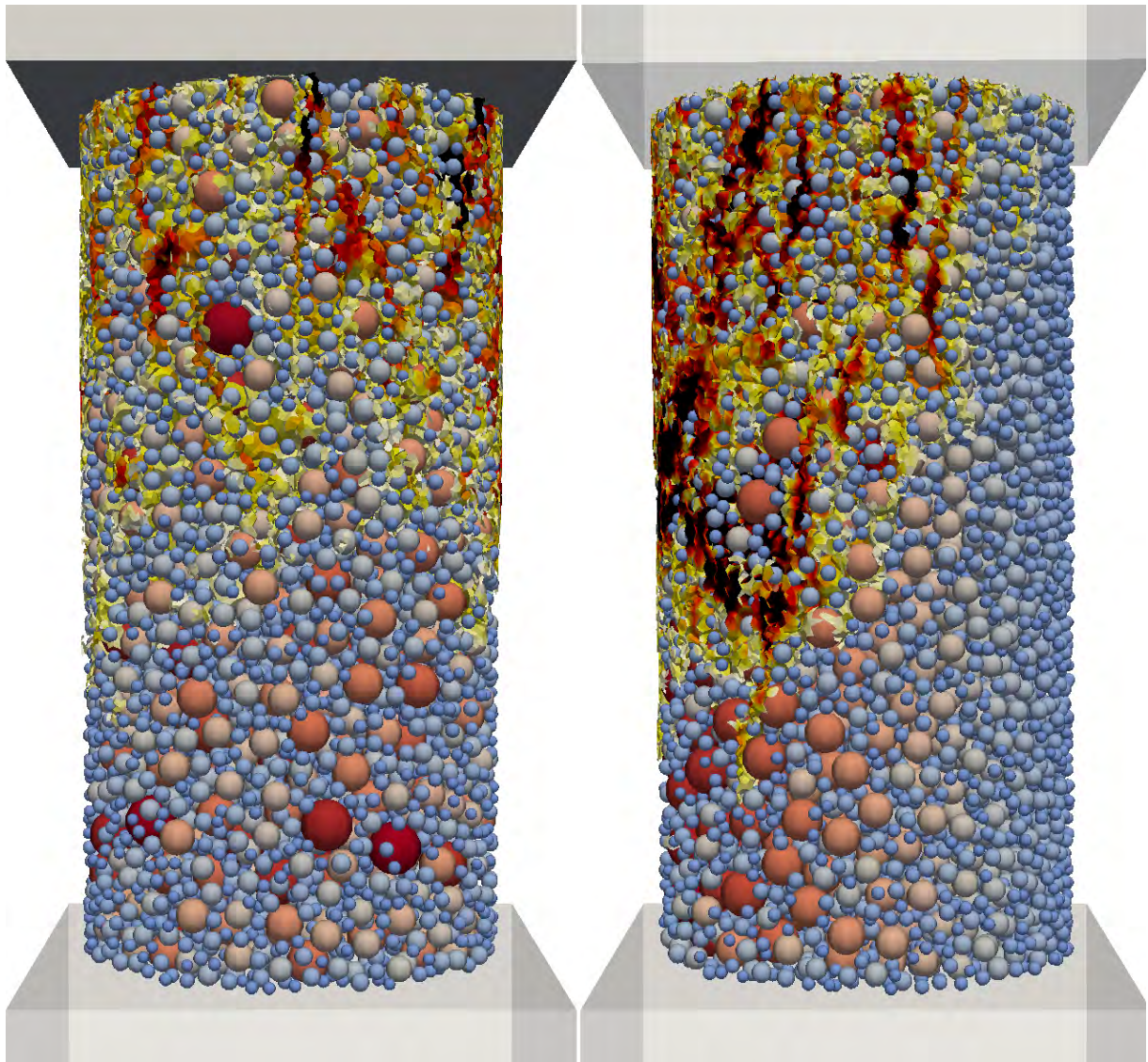


Figure 7.4: Two random LDPM realizations of 3PB experiments governed by the same random field model. Figure by author.

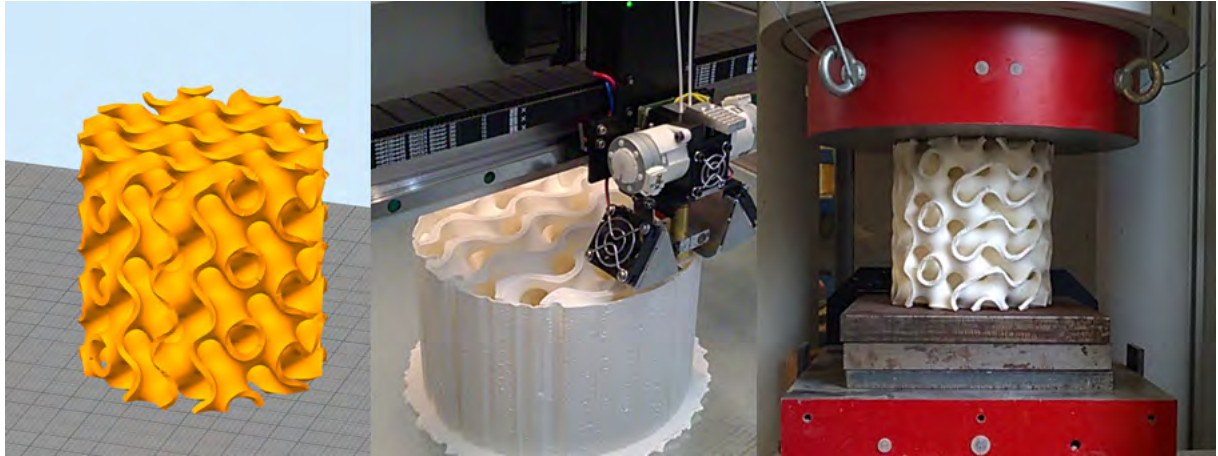


Figure 7.5: Experimental production and testing process of the Gyroid RVE. Figure by author.

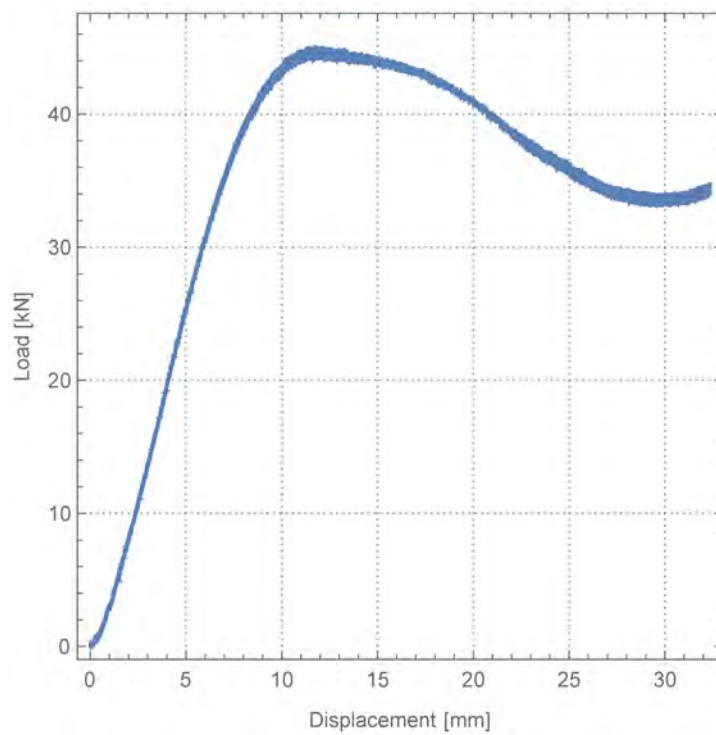


Figure 7.6: Load-displacement diagram of the gyroid sample printed from PLA. Figure by author.



Figure 7.7: Gyroid sample printed from PLA after the compression test. Figure by author.

Part III

Spatial materials

Chapter 8

3D infill patterns

In 3D printing, the structure that is printed inside an object is referred to as infill. It is extruded in a designated pattern and percentage, which is governed by the selected thickness and scale. The infill settings are typically handled by the slicing software and may influence the material usage (weight), strength and print time. Alternatively, the infill patterns may be directly modeled by any general purpose CAD (computer aided design) or computer algebraic system, as has been done in the case of the presented 3D infills (honeycomb is not considered 3D infill), which are not currently available in any slicing software, according to the authors' knowledge. The presented examples and printed test specimens were generated by using the computer algebraic system Mathematica (Wolfram Research) and tested by the engineering simulation software ANSYS [2]. Generally, there are two options on how to generate 3D infills. The first is to apply parametric equations approximating the shape while the second is to copy, rotate and mirror basic building elements. The conventional 2D infill patterns include rectilinear, grid, triangular, wiggle and hexagonal (selected, Figure 8.1).

The 3D patterns were selected from a family of triply periodic minimal surfaces (TPMS) [20, 38], which are known to be invariant under a rank-3 lattice of translations and for having a zero mean curvature (a surface that locally minimizes its area). In the real world, examples of TPMS include some biological structures in nature, block copolymers and electrostatic equipotential surfaces in crystals. According to [13], most TPMS forms exist as an interface between two phases. In particular, a gyroid, Schwarz D and Schwarz P were selected (Figures 8.1 and 8.2).

8.1 Gyroid

The gyroid was first described by NASA scientist A. Shoen in 1970 [38]. In nature, self-assembled gyroid structures can be found in certain surfactant or lipid mesophases or block copolymers [26], inside cells [14] or in biological structural coloration [37], to name the few. The mechanics of a pristine gyroid graphene structure have been recently investigated by [35], who, with respect to engineering applications, pointed out its ultralight nature, outstanding mechanical properties, high surface area, and stable chemical and thermal properties.

The gyroid surface can be trigonometrically approximated by the following equation (implicit surface):

$$\sin x \cos y + \sin y \cos z + \sin z \cos x = 0 \tag{8.1}$$

8.2 Schwarz surfaces

The Schwarz D and P surfaces were first described by H. A. Schwarz and his student E. R. Neovius in the 1880s [39]. Both the D and P surfaces have been considered for prototyping tissue scaffolds with a high surface-to-volume ratio and porosity or compact light-weight fuel cells with high energy density [40, 13].

The Schwarz D surface can be approximated by the following equation:

$$\sin x \sin y \sin z + \sin x \cos y \cos z + \cos x \sin y \cos z + \cos x \cos y \sin z = 0 \quad (8.2)$$

and the Schwartz P surface can be expressed as:

$$\cos x \cos y \cos z = 0 \quad (8.3)$$

The investigations of tailored materials are typically carried out at lower scales, where hierarchical structures are studied due to their exclusive properties, such as ultralight nature, high surface area-to-volume ratio or chemical reaction efficiency. Various applications include drug-eluting devices, water purification filters, or energy-harvesting devices. At the nanoscale, e.g., a 3D printed gyroid with embedded photocatalytic ability was recently described by [17].

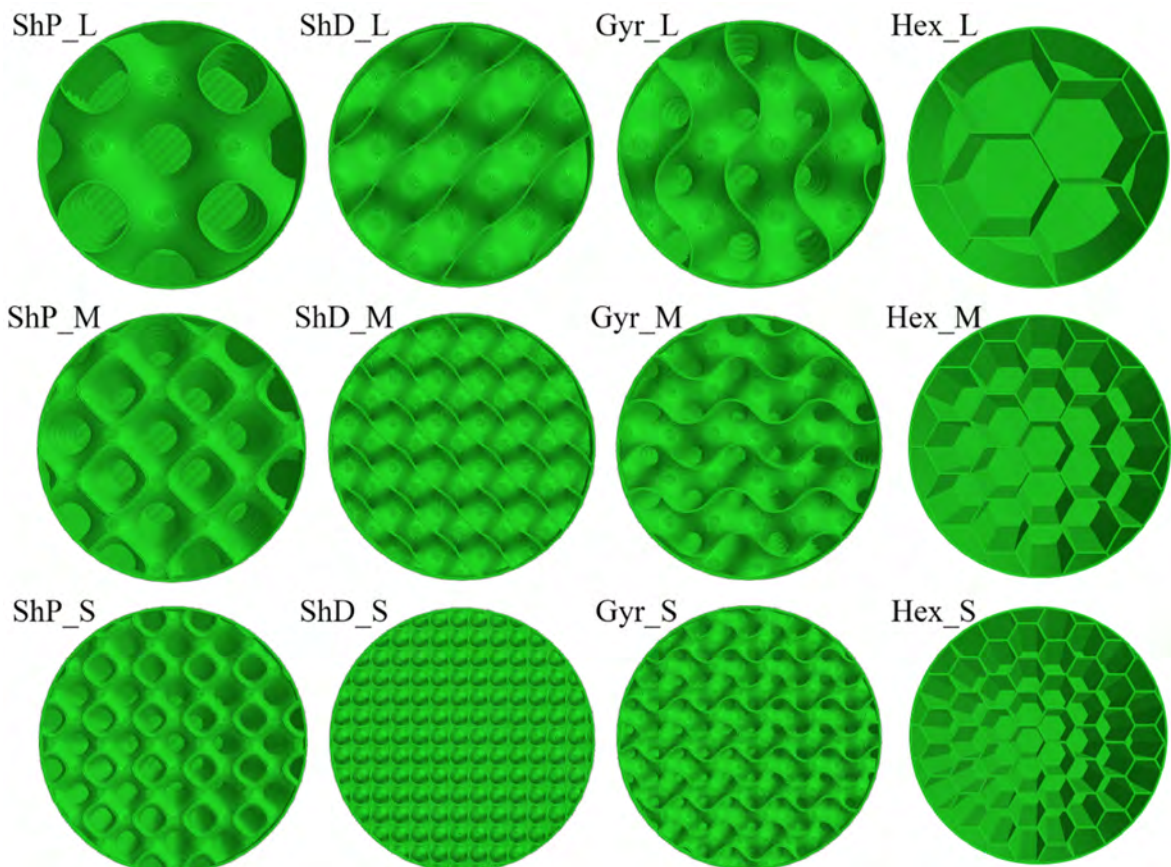


Figure 8.1: Overview of tested 3D and 2D infill alternatives (left to right): Schwarz P, Schwarz D, Gyroid and Hexagonal; and sizes (top to bottom): Large, Medium and Small. Figure by author.

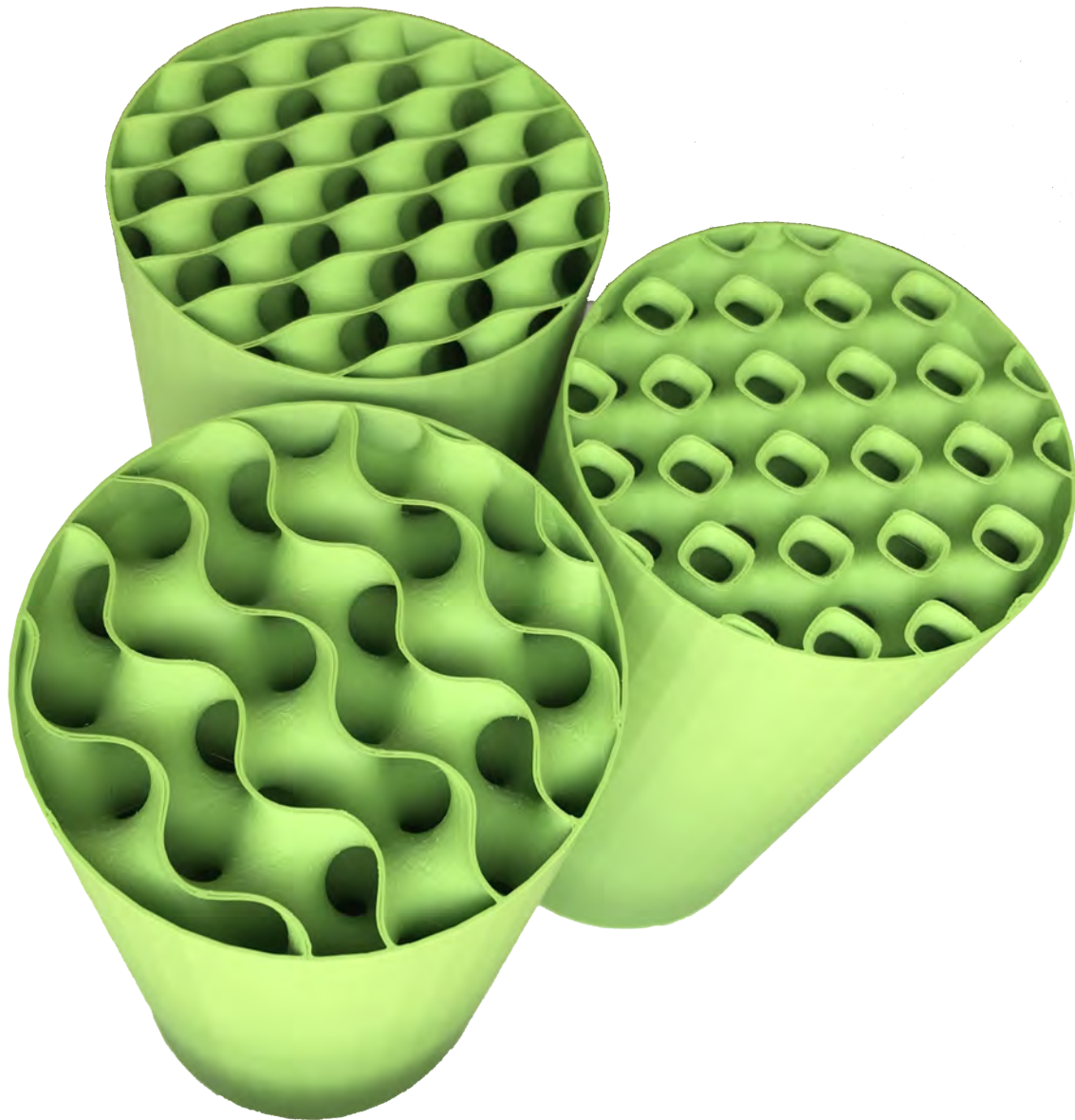


Figure 8.2: Example of 3D printed 3D infill patterns (Schwarz P, Schwarz D and Gyroid at medium scale) generated inside a cylinder. Photographed by author in 2018.

Chapter 9

Experimental investigation

The purpose of the experimental investigation was to analyse the qualitative and quantitative differences in mechanical response between the investigated 3D infill patterns (3 types) in comparison to the reference 2D pattern (honeycomb). This data will serve for the validation of computational models in order to investigate also more complex stress states. By considering 3 length scales per each infill type, 12 combinations of infill patterns (Figure 8.1) have been generated inside a cylinder and 3D printed (Figure 9.4). In case of one gyroid geometry three specimens were printed in order to characterize the inherent production and testing process variability. In total 15 cylinder specimens were tested in a standard compression test configuration (Figure 9.6 right). Part of this chapter originates from a recently published paper in *Materials* [30].

The common properties of all tested cylinders are height (200 mm), diameter (100 mm), constant wall thickness of two perimeters (2 x 0.45 mm extrusion width = 0.9 mm). Unfortunately, the pure infill pattern can not be printed due to limitations in the production process. A bottom solid face is necessary as a stabilizing base, avoiding the otherwise necessary brim, i.e. additional perimeters extending outward from the object. Similarly, the cylindrical jacket is required in order to avoid supports. In order to quantify the potentially confining effect of these required elements extra specimens have been tested (i) without the outside walls, (ii) without bottom face, and (iii) with 0% infill (just cylinder jacket).

The mechanical characterization of the test specimens was carried out by a hydraulic compression testing machine in combination with a 3D digital image correlation (DIC) system (Figure 9.7 b), enabling to record full strain fields and objectively interpret the load-displacement diagrams and stiffness (Figures 10.1 and 10.3). Each compression test was controlled by a prescribed displacement rate with a total displacement limit of 85 mm (0.42 strain).

The tensile characterization of the PLA filament was performed using classical ISO (see [1]) dog bone test specimens, which were sliced according to 3 different strategies, varying infill angle and number of perimeters (Figure 9.5, all 100% infill).

9.1 Production of specimens

All test specimens, i.e. cylinder and dog bone specimens, were printed by the layer-based FDM method from the same batch of PLA filament in order to minimize systematic bias due to production and storage. A serially-produced printer model Prusa i3 MK2 with a 0.4 mm nozzle was used together with the slicing software Simplify3D, as the infills were modeled externally and not generated by the slicing software. The following parameters were considered:

- layer height: 0.15 mm,
- outline/perimeter shells: 2 (x 0.45 mm), including the infill,
- build plate temperature: 55°C,
- printing head temperature: 215°C,
- default printing speed: 2400 mm/min.

Random start points for all perimeters was used in order to avoid a seam which could affect the mechanical properties. This resulted in longer printing time due to significant increase in travel moves. The printing time averaged around 30 hrs per specimen and the weight averaged around 150 grams per specimen.



Figure 9.1: Industrial grade large scale FDM 3D printer Builder 2000. Photographed by the author in 2018.

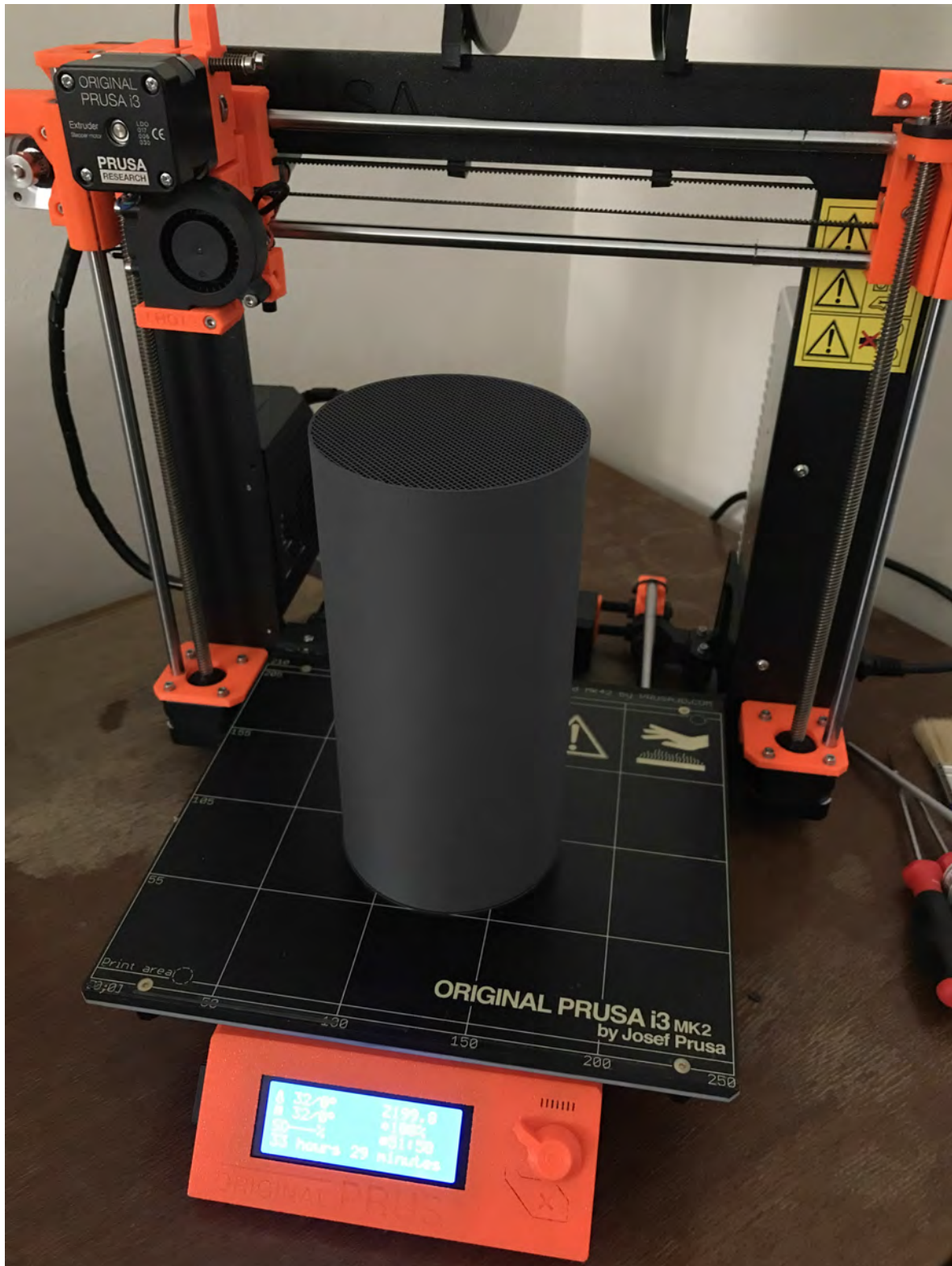


Figure 9.2: Desktop FDM 3D printer Prusa i3 MK2. Photographed by the author in 2018.

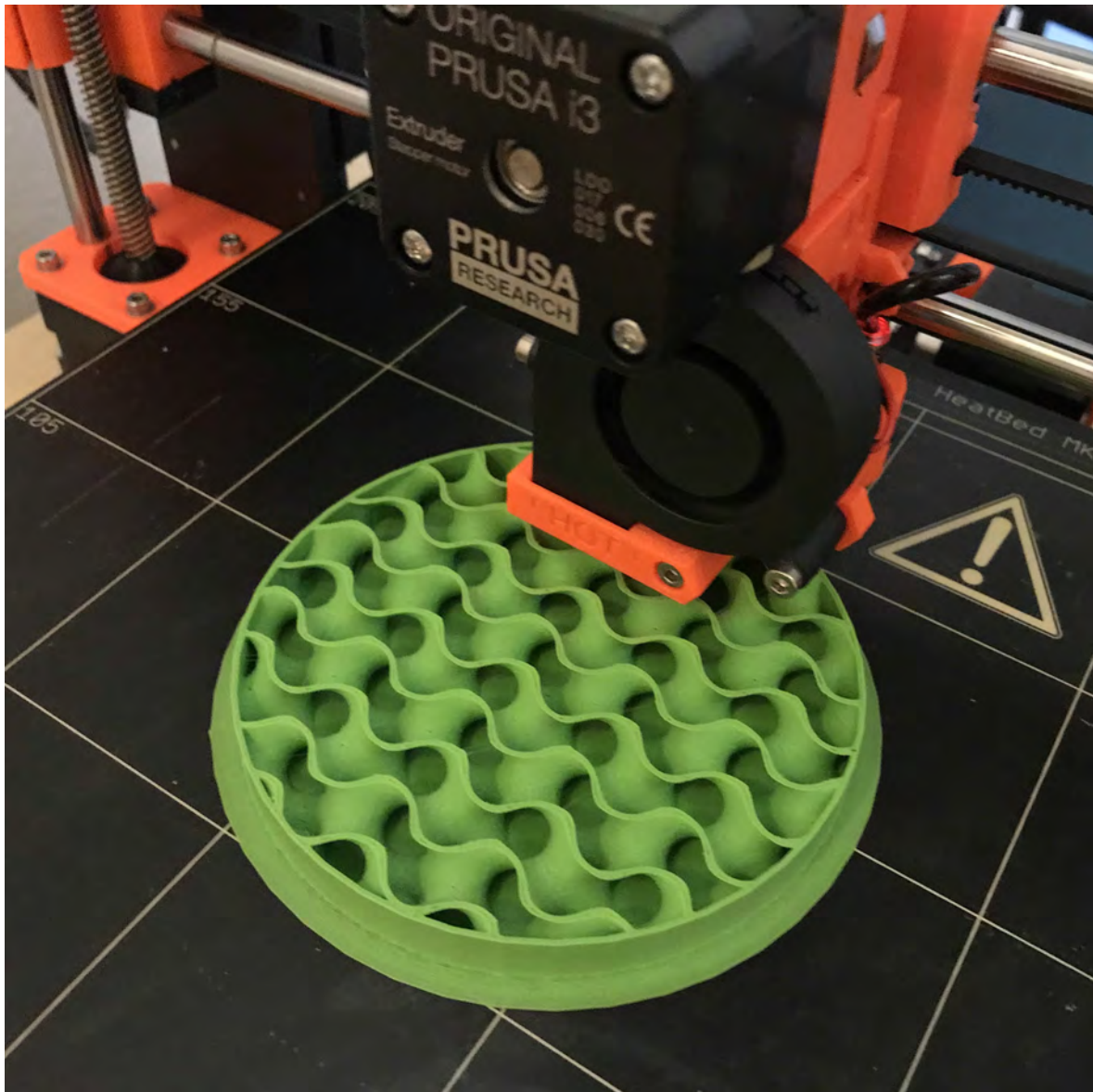


Figure 9.3: Detail of several first layers of gyroid specimen and for increased adhesion a solid bottom face with a brim. Photographed by the author in 2018.

9.2 Physical tests

The mechanical characterization of the cylindrical specimens was carried out by a hydraulic compression testing machine (Figure 9.6). Each compression test was controlled by a prescribed displacement rate with a total displacement limit of 85 mm (0.42 strain). In total, 15 cylinder specimens were tested in a standard compression test configuration (Figure 9.7).

The tensile characterization of the PLA filament was performed using classical ISO (see [1]) dog bone test specimens, which were sliced according to 3 different strategies, varying infill angle and number of perimeters (Figure 9.5, all 100% infill). The associated variability, which is inherent to the production and testing process, has been evaluated for all 3 slicing



Figure 9.4: Sample group of 3D printed specimens from the same filament batch, i.e. same source and storing conditions, in order to eliminate detrimental effects of material degradation and ageing. Photographed by the author in 2018.



Figure 9.5: Different slicing strategies of material characterization based on ISO tensile test specimens (Top: DB 00, center: DB 90 and bottom: DB Hy). Figure by author.

strategies by printing and testing 3 identical specimens. All 12 DB specimens, some damaged by the testing, are shown in Figures 9.12 (DB 00), 9.13 (DB 90) and 9.14 (DB Hy). In is

not surprising that the slicing strategy DB 00 resulted in most performing specimen, as the manufacturing process (extrusion orientation) has been aligned with the loading direction and principal stress. This slicing strategy, however, is not typical for standard use, where a number of several perimeters usually encloses the filled region, which is sliced in not only 1 direction, but more directions, in a periodic consecutive order. Due to large number of established slicing strategies, which are specific to expert judgement and printed object, it was not the intention of the author to test all possible slicing strategies, but to rather demonstrate the orthotropic principle of layer-based printing and the associated variability.

All tested specimens were were sprayed with a black and white paint to create a high-contrast random pattern. This enabled the automated and reliable shape measurements with DIC system 9.7.

Selected deformed specimens from the compression test are shown in Figures 9.8, 9.9, 9.10 and 9.11, where the failure mechanism can be observed at various scales for the reference 2D hexagonal infills and the 3D infills.

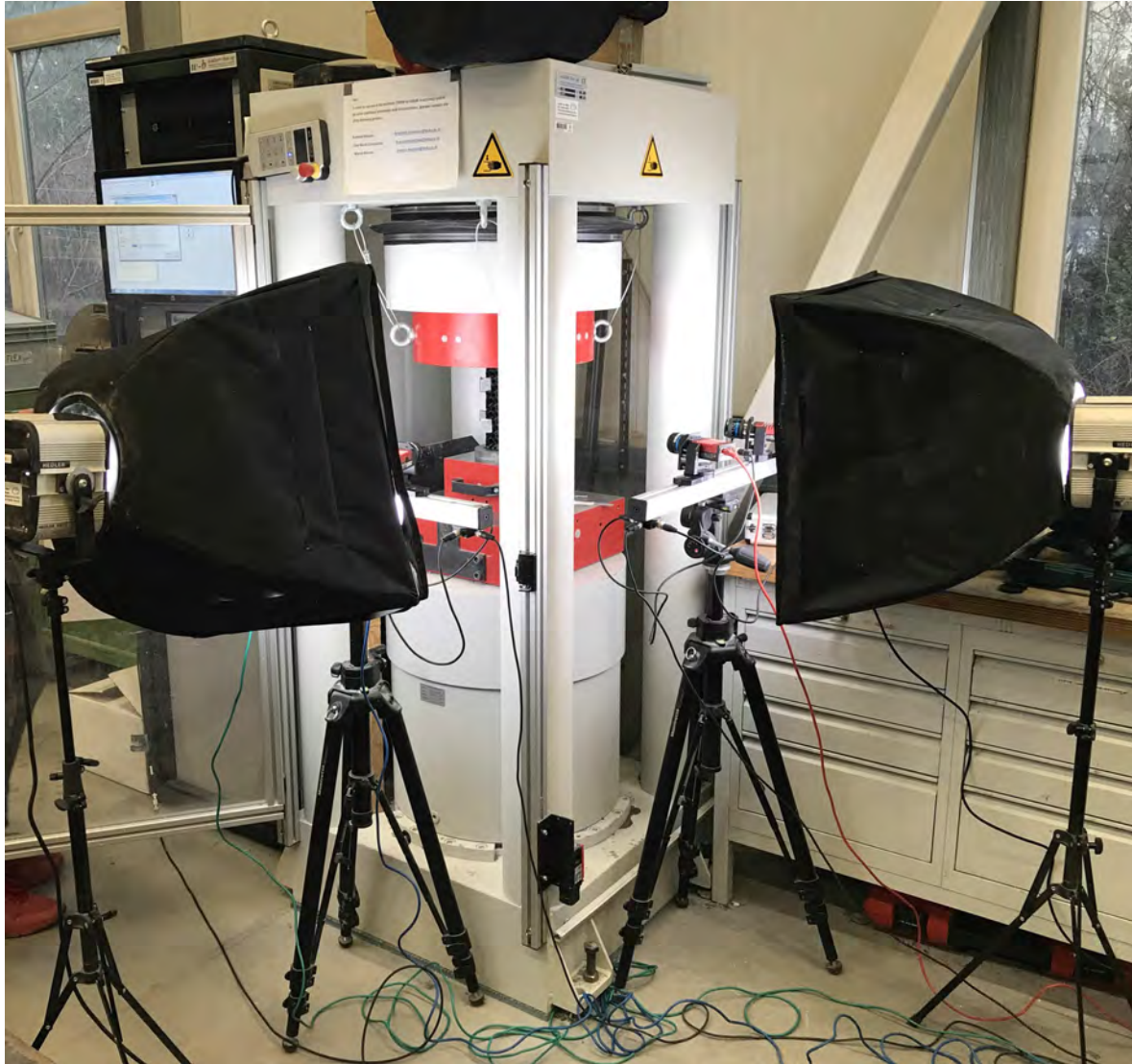


Figure 9.6: Hydraulic compression testing machine controlled by a prescribed displacement rate in combination with a 3D digital image correlation (DIC) system enabling to record full strain fields and objectively interpret the load-displacement diagrams and stiffness. Photographed by the author in 2018.

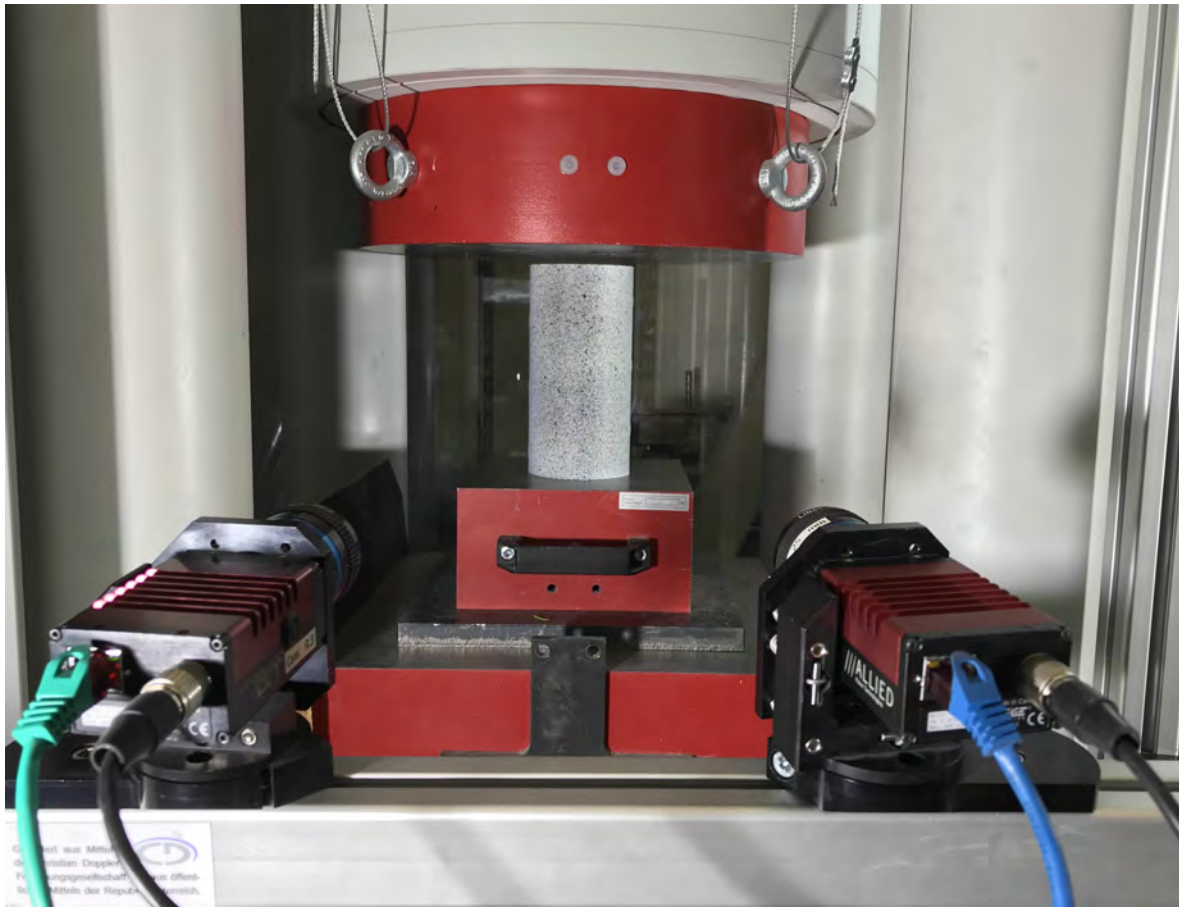


Figure 9.7: Detail of the hydraulic compression test setup and visible high-contrast random pattern applied to the compressed specimen's surface for automated and reliable shape measurements with DIC. Photographed by the author in 2018.



Figure 9.8: Sample realizations of cylinder compression tests with 3 scales of reference 2D honeycomb infill. Photographed by the author in 2018.



Figure 9.9: Sample realizations of cylinder compression tests with 3 scales of 3D gyroid infill. Photographed by the author in 2018.



Figure 9.10: Sample realizations of cylinder compression tests with 3 scales of 3D Schwarz D infill. Photographed by the author in 2018.



Figure 9.11: Sample realizations of cylinder compression tests with 3 scales of 3D Schwarz P infill. Photographed by the author in 2018.



Figure 9.12: Three realizations of ISO dogbone specimens sliced according to DB 00 after the tensile test. Photographed by the author in 2018.



Figure 9.13: Three realizations of ISO dogbone specimens sliced according to DB 90 after the tensile test. Photographed by the author in 2018.



Figure 9.14: Three realizations of ISO dogbone specimens sliced according to DB Hy after the tensile test. Photographed by the author in 2018.

Chapter 10

Results

The results of the cylinder compression tests are presented and discussed at section *Experimental* and relate to the performance of various infills (metamaterials, 3D materials), while the results of the dog bone tensile tests are presented in the section *Numerical*, where they relate to the actual PLA material and anisotropy of 100% infill resulting from different slicing strategy. The latter is used to calibrate the nonlinear PLA material model for the preliminary finite element modelling framework, which is validated by the former. The numerical model will consequently serve for the design of component-scale experiments, such as the presented branching structure (Figures 6.1 and 6.2), and as a proof of concept is presented here with limited details.

10.0.1 Experimental

The performance of the tested 2D and 3D infills at various scales (densities or weights) has been quantitatively evaluated in terms of stiffness and peak load in Figure 10.1. Here, various functional forms have been considered for the scaling laws, however, linear interpolation seemed most appropriate. The linear trend lines show that both in terms of stiffness and peak load, the 2D hexagonal infill outperformed the tested 3D infills, which is not surprising considering that the extrusion axis of the pattern is aligned with the axis of the macroscopic member (cylinder) and the principal stress field. Note that such conditions are very specific and generally not possible due to geometrical reasons and the multitude of possible loading scenarios in real world applications, such as presented in the example of a branching structure (Figures 6.1 and 6.2). Among the investigated 3D infills the Schwarz P surface is the least performant structure, while the Schwarz D and Gyroid perform similarly well.

The associated variability, which is inherent to the production and testing process, has been characterized based on three identical Gyroid specimens (Figure 10.1, green crosses “Repet”.) in table 1. For a reference, the confinement itself (specimen with 0% infill, Figure 10.1, turquoise x mark “Empty”) has been tested, together with specimens without confinement walls (difficult to print without supports) and with confinement walls but without the bottom face (0.54% difference).

The recorded load-displacement diagrams and strain fields from DIC finally serve for

Table 10.1: Production and testing process variability based on 3 identical Gyroid specimens (* coefficient of variation).

	Weight	Peak load	Stiffness
Mean	217.47 g	15.84 kN	174.43
COV*	1.87%	5.29%	12.92%

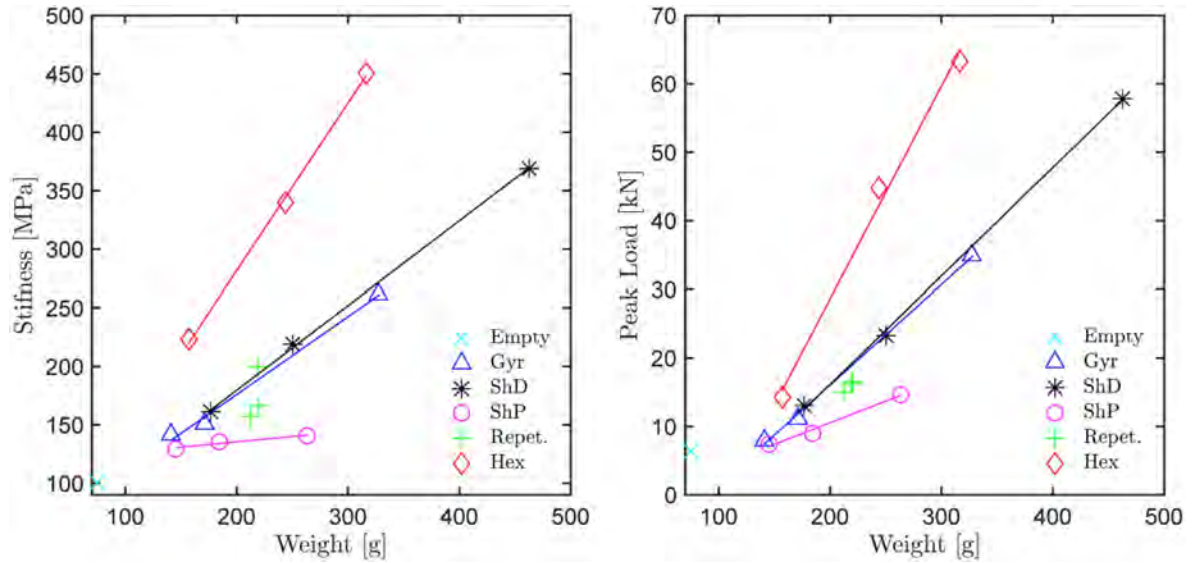


Figure 10.1: Mechanical performance of tested lattices as a function of weight: stiffness and peak load capacity. Figure by author.

analysing qualitatively differences in ductility, strain periodicity resulting from the hierarchical lattice, and a sequential collapse with damage localization (Figures 10.2 and 10.3). Although all investigated specimens exhibited large deformation capacity with strains of up to 0.42 owing to the infill patterns and the chosen PLA filaments, the specimens with 3D infills exhibited smoother strain fields in general, especially compared to the 2D hexagonal infills. This effect can be attributed to local buckling and stress concentrations which are significantly reduced by 3D infills (shorter buckling length) and can also be observed in the computational simulation results (Figure 10.5). The sensitivity of the layer-based FDM process to slicing strategy and build orientation based on tensile dog bone specimens is statistically evaluated in Figure 10.4. Finally, that data serves as input for the calibration of non-linear material models.

10.0.2 Numerical

The classical cylinder compression test results show, among others, that when a 2D infill pattern is aligned with the principal stress orientation, the 2D infill may outperform the 3D infill. The general design, however, typically involves more complex shapes and boundary conditions, which cannot be easily approximated by classical mechanical tests, and where there is no preferable extrusion orientation for 2D infills. In such cases, 3D infills may represent more efficient alternatives to classical 2D infills, if properly understood and designed. This clearly cannot be done without a computational model (e.g. FEM) calibrated and validated by data from classical physical experiments. These should entail compression and fracture tests, and account for any anisotropy due to printing artifacts.

In a first approach we characterize the rather complex anisotropic behavior associated with layer-based production processes by simple tensile tests on standard “dog bone” (DB) specimens [1]. As the slicing strategy and build orientation may significantly affect the mechanical performance, the DB specimens have been sliced in 3 ways according to (Figure 9.5) with three repetitions for each scenario to generate a minimum of statistical insights. The results

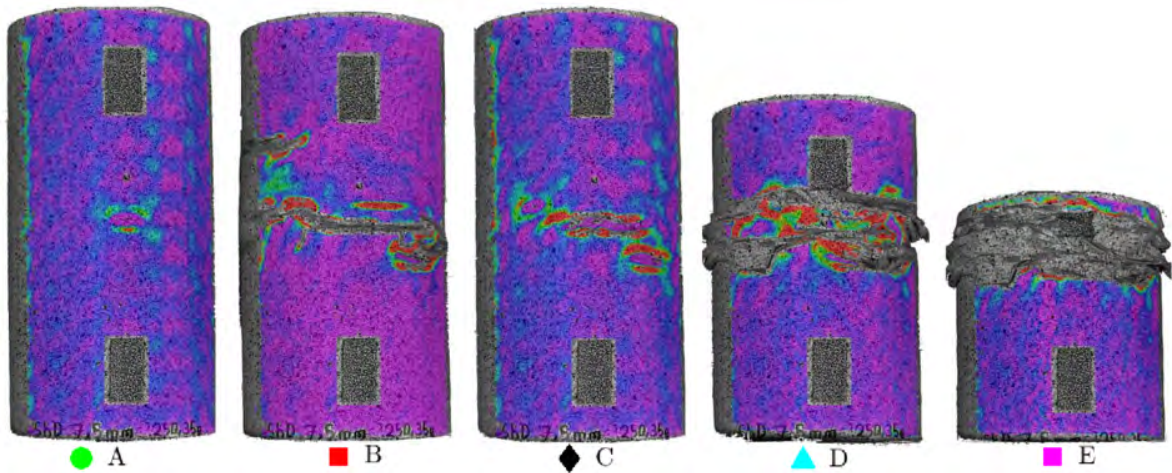


Figure 10.2: ShD M: illustration of sequential collapse using damage localisation based on 5 DIC strain fields (Lagrange, horizontal component, A to E) mapped to black and white photos of the compressed specimens. Figure by author.

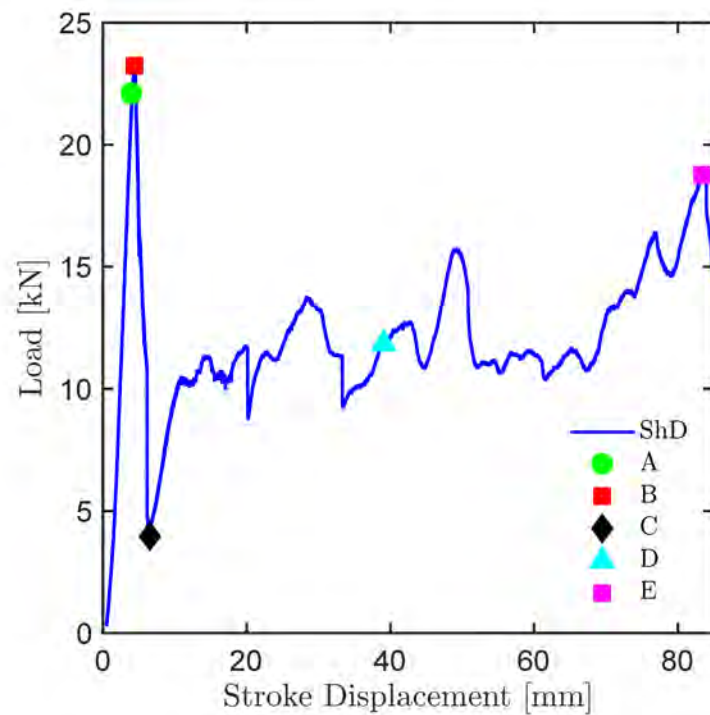


Figure 10.3: ShD M: illustration of sequential collapse using Load-Displacement diagram and positions of 5 DIC strain fields (A to E) from (fig. 10.2). Figure by author.

are shown in Figure 10.4. Here, the slicing strategy DB_00 refers to the case where the extrusion direction was aligned with the loading direction (no perimeters used), providing maximum load capacity, DB_90 is the most ineffective strategy, where the extrusion direction is normal to the loading direction and no perimeters are used. DB_Hy refers to a more tra-

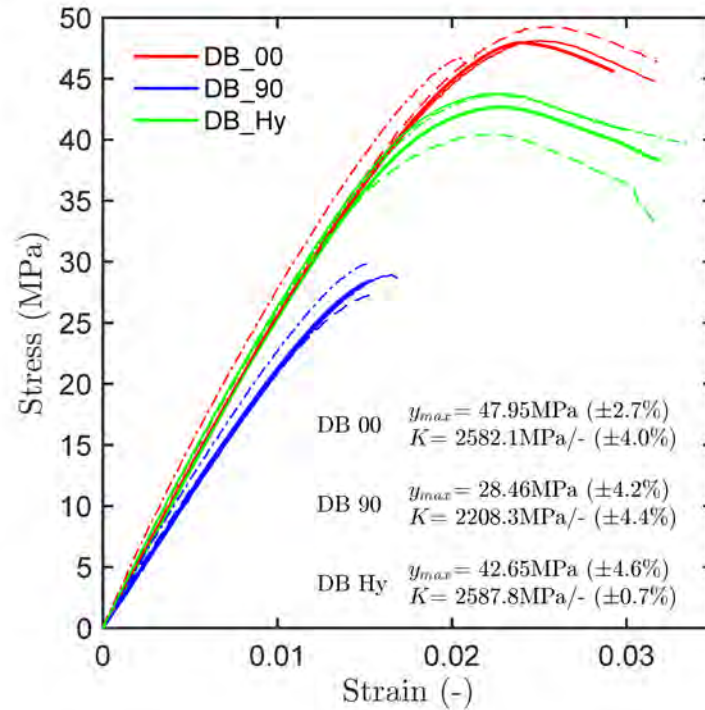


Figure 10.4: Material characterization based on ISO tensile test specimens and 3 different slicing strategies for nonlinear material model. Figure by author.

ditional slicing strategy, where 6 perimeters are used and the remaining volume is sliced as a DB_00 and DB_90 repetitive sequence, i.e. each infill layer has an infill angle normal to that of neighboring layers. At this point further material tests characterizing e.g. the interface properties between layers in mode I and mode II have not been performed.

The stress-strain relationships from the ISO tensile tests (DB) have been used to formulate a custom nonlinear material model for PLA for preliminary static structural analysis (ANSYS® Mechanical™) in order to simulate the physical experiments. The number of nodes amounts to approx. 1.2×10^6 and the elapsed run-time amounts to approx. 50 hours at a standard workstation computer with 4 cores operating at 4 GHz with 16 GB RAM. With the exception of the material properties all other solution parameters were automatically set within mechanical physics preference.

The numerical results coincide with the experimental data by approx. +/- 10%. An example of a simulated cylinder with gyroid medium infill (Gyr_M) can be seen in Figure 10.5. The external surface exhibits periodic features in the strain field, similar to those observed by digital image correlation in the actual experiments. These are unique to the gyroid infill type. Unlike the DIC results that are limited to the surface the numerical analysis provide interesting insights into the sequential collapse mechanism by allowing to trace also the porous inner structure hidden to the optical DIC system.

In a next step the computational model may further be used to explore more efficiently the high-dimensional design space with respect to different geometries, lattice types, scales, and associated parameters.

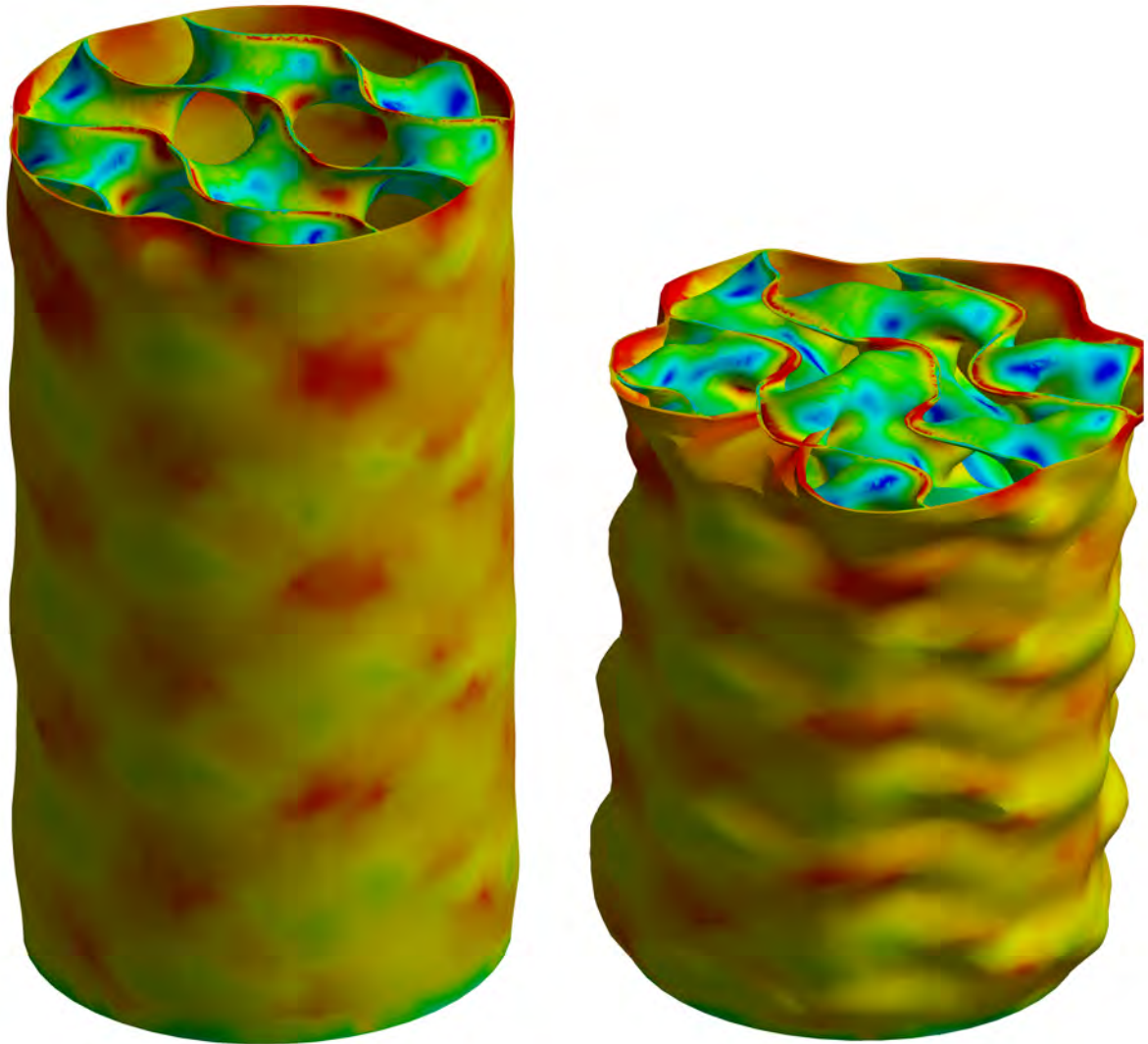


Figure 10.5: Periodic strain fields from the preliminary FEM analysis and different load levels. Figure by author.

10.0.3 Vacuum coating

The PLA material, a polymer from renewable resources, such as corn or potato starch, is known to be sensitive to exposure conditions. Absorption of moisture over time allows hydrolysis of the ester bond to occur, a primary mode of degradation.

The degradation rate highly depends factors including microstructure, part geometry and thickness, moisture and heat exposure, the presence of microbes, etc.

Since the use of PLA for durable applications requires the assessment of long-term performance, an experimental vacuum coating has been conducted on a porous gyroid structure without the confinement jacket (Figure 10.6). The vacuum coating is preferential mode of surface finish, because of absence of elevated temperature during the process.

This result has been conducted within the applied research project *Vacuum coating system for rapid prototyping*. The author of this thesis is the main applicant of this project, the aim of

which is to develop a unique vacuum coating system for rapid prototyping (VPAT), which will strengthen the position of both applicants in Industry 4.0 and increase their competitiveness. The research potential in the field of rapid prototyping, already available to applicants, will be further developed and used to solve applied research (BUT in Brno) and sub-deliveries to automotive and other industries (ČEGAN s.r.o.). At the same time, it is expected that an influx of technologically demanding contracts that can not be solved without the proposed vacuum coating system.

In regard to the application of highly porous structures and known materials for 3D printing, surface finish is an important durability aspect, where the traditional surface finishing options are not longer effective due to the presence of hardly accessible voids. Gravity effects are known to cause problems when heat-treating or soaking the specimens.

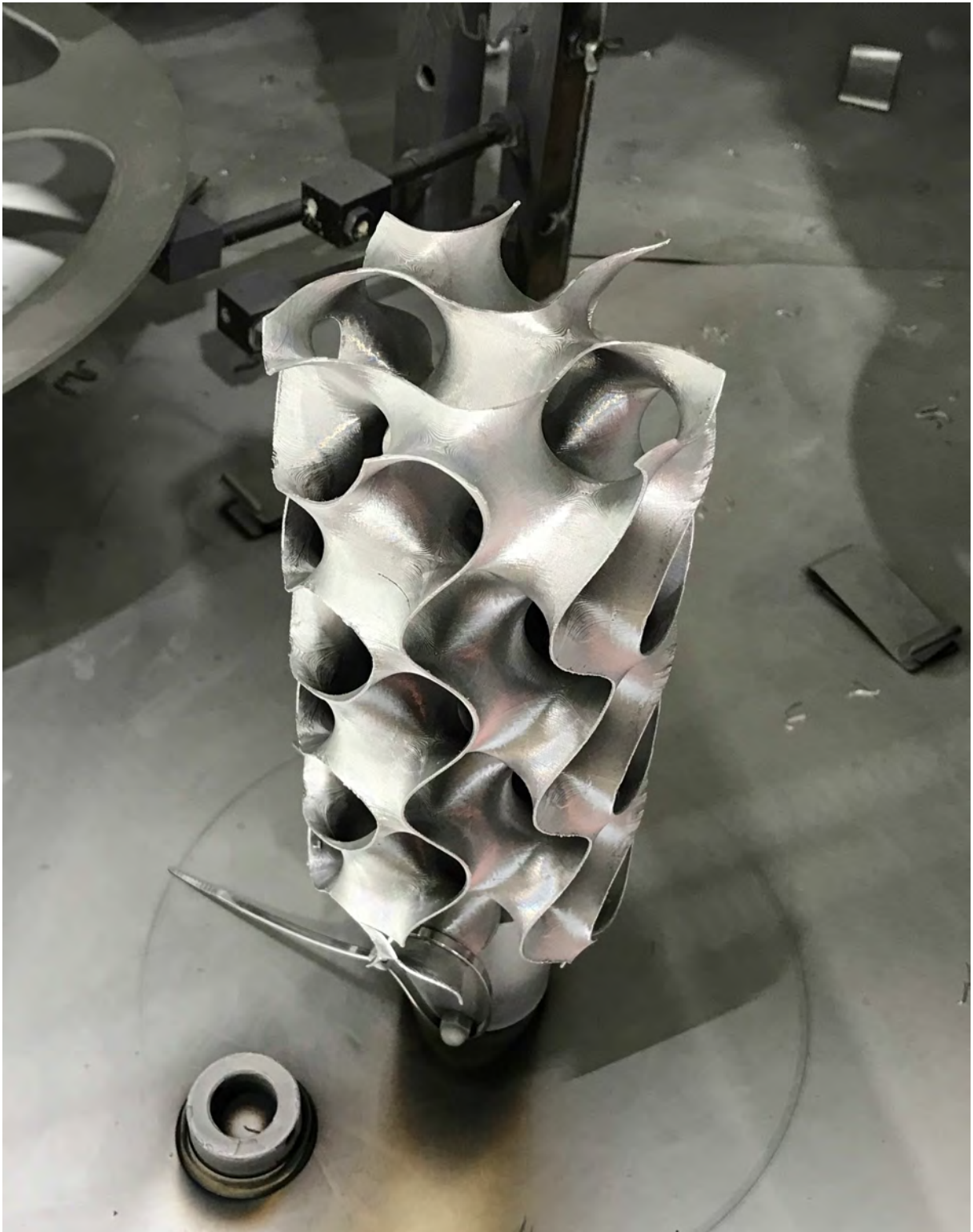


Figure 10.6: Vacuum coating of the gyroid surface without the cylindrical confinement jacket. Photographed by the author in 2018.

Chapter 11

Discussion

It is well known that the structural performance of layer-based FDM printouts can be significantly anisotropic (sensitive to build orientation). By properly aligning the filament deposition orientation and structural action, the structural performance may increase by up to 60%.

This may be sufficient for simply supported and loaded components, such as the tested cylinder mimicking a column under centric compression. However, for complex streamlined structural components such as the presented branching structures (Figure 6.1), the (organic) shape of which is often governed by optimization (generative design), it is not possible anymore to align the infill orientation with the direction of maximum principal stresses.

Therefore, a variety of (bio-inspired) 3D infills have been proposed and analyzed as a layer-based FDM-compatible alternative to currently used 2D infills. Note that the presented 3D infills can only be (continuously) fabricated by 3D printing (at the presented scales). Thus, any attempt to actually characterize their mechanical performance had to wait for more than hundred years for the AM to fully develop.

Among the most structurally important aspect of the presented 3D infills is the double curvature which provides the required stability (stiffness). Moreover, the triply periodic minimal surface of the gyroid (3D infill), known for its constant curvature, has no planes of symmetry and no embedded straight lines, which is useful when filling the above-mentioned complex geometry regions.

The 2D infills, such as rectangular or hexagonal grid, are not generally suitable for structural applications with complex 3D geometry due to the resulting anisotropy (sensitivity to the orientation of the 2D lattice). However, in case of simply loaded and supported classical specimens, 2D infills may outperform 3D infills.

If 3D printing is the future of construction in civil engineering, then the structural members no longer have to be limited to rectilinear and solid bodies. In these cases a multi-scale approach in the design optimization, which will lead in some cases to organic streamlined structures with bio-inspired infill patterns, will bring many new opportunities. These will be trailed by challenges, as the current design guidelines, safety concepts, and performance indicators will have to be thoroughly reviewed and possibly adapted for AM.

Chapter 12

Conclusion and outlook

The particular results of the mechanical characterization of the 2D and 3D infills can be summarized as following:

- Stiffness (modulus) results obtained by digital image correlation (DIC) show a linear scaling law with infill density, COV of 12.92% and equally performant Gyroid and Schwarz D.
- Load capacity (peak stress) results show a linear scaling law, COV of 5.92% and equally performant Gyroid and Schwarz D.
- All investigated specimens exhibit ductile behavior (from load-displacement diagrams) and the specimens with 3D infills smooth strain periodicity without stress concentrations (when compared to 2D hexagonal infills).
- The sensitivity to slicing strategy and build orientation was evaluated on a dog bone tensile test specimens, resulting in up to 60% difference and relatively small scattering (COV ranging from 0.7 to 4.6%).

The preliminary nonlinear FEM analysis calibrated by the tensile dog bone specimens shows a good qualitative agreement with the experimental results in terms of peak load, stiffness and periodic strain fields. However, the calculations are extremely computationally expensive making any systematic upscaling to large structures an unfeasible proposition.

Based on the presented theoretical arguments and experiments it can be assumed that custom 3D infill patterns may be an interesting alternative to classical (2D) infills in additive manufacturing if (i) general stress states are likely to occur, or (ii) in case of complex geometries. 3D infills avoid introducing macroscopic anisotropy by additive manufacturing while still achieving large weight reductions.

Lightweight generative multi-scale design can be applied at architectural scales, potentially offering additional benefits in terms of tuned thermal, acoustic, static or dynamic properties, including e.g. passive evaporative cooling similar to how buildings were cooled in ancient Oman. This would, however, require a highly scalable multi-physics simulation framework to support the representation and simulation of material structure and evolution across multiple length and time scales, such as the Digital Material concept.

Bibliography

- [1] ISO, 527-2, Plastics – determination of tensile properties, part 2. 2012.
- [2] ANSYS® Mechanical™ Release 19.1. Computer program, 2018.
- [3] IDEA StatiCa. Computer program, 2018.
- [4] Wolfram Research, Wolfram Mathematica Release 11.3.0. Computer program, 2018.
- [5] Amir, O.: A topology optimization procedure for reinforced concrete structures. *Computers & Structures*, ročník 114, 2013: s. 46–58.
- [6] Benvenuti, S.; Ceccanti, F.; De Kestelier, X.: Living on the moon: topological optimization of a 3D-printed lunar shelter. *Nexus Network Journal*, ročník 15, č. 2, 2013: s. 285–302.
- [7] Brekelmans, W.; Poort, H.; Slooff, T.: A new method to analyse the mechanical behaviour of skeletal parts. *Acta Orthopaedica Scandinavica*, ročník 43, č. 5, 1972: s. 301–317.
- [8] Camacho, D. D.; Clayton, P.; O'Brien, W.; aj.: Applications of Additive Manufacturing in the Construction Industry—A Prospective Review. In *ISARC. Proceedings of the International Symposium on Automation and Robotics in Construction*, ročník 34, Vilnius Gediminas Technical University, Department of Construction Economics & , 2017.
- [9] COBOD: Gantry versus robotic arm based 3d construction printers. *webpage cobod.com*, 2018.
- [10] Cusatis, G.; Pelessone, D.; Mencarelli, A.: Lattice discrete particle model (LDPM) for failure behavior of concrete. I: Theory. *Cement and Concrete Composites*, ročník 33, č. 9, 2011: s. 881–890.
- [11] Farah, S.; Anderson, D. G.; Langer, R.: Physical and mechanical properties of PLA, and their functions in widespread applications—A comprehensive review. *Advanced drug delivery reviews*, ročník 107, 2016: s. 367–392.
- [12] Gibson, I.; Rosen, D.; Stucker, B.: *Additive Manufacturing Technologies: 3D Printing, Rapid Prototyping, and Direct Digital Manufacturing*. SpringerLink : Bücher, Springer New York, 2014, ISBN 9781493921133.
URL <https://books.google.cz/books?id=0PGbBQAAQBAJ>
- [13] Han, S. C.; Choi, J. M.; Liu, G.; aj.: A Microscopic Shell Structure with Schwarz's D-Surface. *Scientific reports*, ročník 7, č. 1, 2017: str. 13405.
- [14] Hyde, S.; Blum, Z.; Landh, T.; aj.: *The language of shape: the role of curvature in condensed matter: physics, chemistry and biology*. Elsevier, 1996.

- [15] Ishida, T.; Kishi, T.; Maekawa, K.: *Multi-scale modeling of structural concrete*. Crc Press, 2014.
- [16] Izard, J.-B.; Dubor, A.; Hervé, P.-E.; aj.: Large-scale 3D printing with cable-driven parallel robots. *Construction Robotics*, ročník 1, č. 1-4, 2017: s. 69–76.
- [17] Jo, W.; Yoon, B. J.; Lee, H.; aj.: 3D Printed Hierarchical Gyroid Structure with Embedded Photocatalyst TiO₂ Nanoparticles. *3D Printing and Additive Manufacturing*, ročník 4, č. 4, 2017: s. 222–230.
- [18] Jokic, S.; Novikov, P.; Maggs, S.; aj.: Minibuilders. *Architectural principles, tools, and processes. Digital Vernacular*, 2015: s. 259–265.
- [19] Kading, B.; Straub, J.: Utilizing in-situ resources and 3D printing structures for a manned Mars mission. *Acta Astronautica*, ročník 107, 2015: s. 317–326.
- [20] Karcher, H.: The triply periodic minimal surfaces of Alan Schoen and their constant mean curvature companions. *Manuscripta mathematica*, ročník 64, č. 3, 1989: s. 291–357.
- [21] Keating, S. J.; Leland, J. C.; Cai, L.; aj.: Toward site-specific and self-sufficient robotic fabrication on architectural scales. *Science Robotics*, ročník 2, č. 5, 2017: str. eaam8986.
- [22] Krč, R.; Podroužek, J.; Wan-Wendner, R.: From slender columns to branching structures. In *Computational Modelling of Concrete Structures: Proceedings of the Conference on Computational Modelling of Concrete and Concrete Structures (EURO-C 2018), February 26-March 1, 2018, Bad Hofgastein, Austria*, CRC Press, 2018, str. 165.
- [23] Lim, S.; Buswell, R. A.; Le, T. T.; aj.: Developments in construction-scale additive manufacturing processes. *Automation in construction*, ročník 21, 2012: s. 262–268.
- [24] Liu, J.; Yu, H.: Concurrent deposition path planning and structural topology optimization for additive manufacturing. *Rapid Prototyping Journal*, ročník 23, č. 5, 2017: s. 930–942.
- [25] Lloret, E.; Shahab, A. R.; Linus, M.; aj.: Complex concrete structures: merging existing casting techniques with digital fabrication. *Computer-Aided Design*, ročník 60, 2015: s. 40–49.
- [26] Longley, W.; McIntosh, T. J.: A bicontinuous tetrahedral structure in a liquid-crystalline lipid. *Nature*, ročník 303, č. 5918, 1983: str. 612.
- [27] Mahasenan, N.; Smith, S.; Humphreys, K.: -The Cement Industry and Global Climate Change: Current and Potential Future Cement Industry CO₂ Emissions. In *Greenhouse Gas Control Technologies-6th International Conference*, Elsevier, 2003, s. 995–1000.
- [28] Najam, A.: World Business Councilfor Sustainable Development: The Greening of Business or a Greenwash? In *Yearbook of International Cooperation on Environment and Development 2003-04*, Routledge, 2013, s. 69–81.
- [29] Palmieri, V.; De Lorenzis, L.: Multiscale modeling of concrete and of the FRP–concrete interface. *Engineering Fracture Mechanics*, ročník 131, 2014: s. 150–175.

- [30] Podroulílek, J.; Marcon, M.; NinÄŤeviÄŤ, K.; aj.: Bio-Inspired 3D Infill Patterns for Additive Manufacturing and Structural Applications. *Materials*, ročník 12.3, 2019: str. 499.
- [31] Podrouzek, J.; Bucher, C.; Deodatis, G.: Identification of critical samples of stochastic processes towards feasible structural reliability applications. *Structural Safety*, ročník 47, 2014: s. 39–47.
- [32] Podroušek, J.; Strauss, A.; Bergmeister, K.: Robustness-based performance assessment of a prestressed concrete bridge. *Structural Concrete*, ročník 15, č. 2, 2014: s. 248–257.
- [33] Podroušek, J.; Vorel, J.; Cusatis, G.; aj.: Imposed Correlation Between Random Field and Discrete Particle Placement. In *14th International Probabilistic Workshop*, Springer, 2017, s. 245–252.
- [34] Podroušek, J.; Wan-Wendner, R.: Uncertainty analysis of the power law extrapolation techniques for adhesive anchors. *Structural Concrete*, 2018.
- [35] Qin, Z.; Jung, G. S.; Kang, M. J.; aj.: The mechanics and design of a lightweight three-dimensional graphene assembly. *Science advances*, ročník 3, č. 1, 2017: str. e1601536.
- [36] Rael, R.; Fratello, V.: *Printing Architecture: Innovative Recipes for 3D Printing*. Princeton Architectural Press, 2018, ISBN 9781616897475.
URL <https://books.google.cz/books?id=SoNaDwAAQBAJ>
- [37] Saranathan, V.; Osuji, C. O.; Mochrie, S. G.; aj.: Structure, function, and self-assembly of single network gyroid (I4132) photonic crystals in butterfly wing scales. *Proceedings of the National Academy of Sciences*, ročník 107, č. 26, 2010: s. 11676–11681.
- [38] Schoen, A. H.: Infinite periodic minimal surfaces without self-intersections. 1970.
- [39] Schwarz, H. A.: *Gesammelte mathematische abhandlungen*, ročník 260. American Mathematical Soc., 1890.
- [40] Shin, J.; Kim, S.; Jeong, D.; aj.: Finite element analysis of Schwarz P surface pore geometries for tissue-engineered scaffolds. *Mathematical Problems in Engineering*, ročník 2012, 2012.
- [41] Standard, A.: ISO/ASTM 52900: 2015 Additive manufacturing-General principles-terminology. *ASTM F2792-10e1*, 2012.
- [42] Stromberg, L. L.; Beghini, A.; Baker, W. F.; aj.: Application of layout and topology optimization using pattern gradation for the conceptual design of buildings. *Structural and Multidisciplinary Optimization*, ročník 43, č. 2, 2011: s. 165–180.
- [43] Tam, K.-M. M.; Mueller, C. T.: Additive Manufacturing Along Principal Stress Lines. *3D Printing and Additive Manufacturing*, ročník 4, č. 2, 2017: s. 63–81.
- [44] Tymrak, B.; Kreiger, M.; Pearce, J. M.: Mechanical properties of components fabricated with open-source 3-D printers under realistic environmental conditions. *Materials & Design*, ročník 58, 2014: s. 242–246.

-
- [45] Vořechovská, D.; Podroužek, J.; Chromá, M.; aj.: Modeling of chloride concentration effect on reinforcement corrosion. *Computer-Aided Civil and Infrastructure Engineering*, ročník 24, č. 6, 2009: s. 446–458.
- [46] Wan-Wendner, R.; Podroužek, J.: Robust Power Law Extrapolation for Adhesive Anchors under Sustained Load. *ACI Structural Journal*, ročník 116, č. 1, 2019.
- [47] Wang, X.; Yang, Z.; Yates, J.; aj.: Monte Carlo simulations of mesoscale fracture modelling of concrete with random aggregates and pores. *Construction and Building Materials*, ročník 75, 2015: s. 35–45.

List of Figures

2.1	The entire shelter was assembled by 6-axis robotic arm, which also formatted each individual wooden beam (Masia Can Valldaura, Barcelona, Spain). Photographed by the author in 2018.	20
4.1	Science centre and comprehensive civil engineering research institution AdMaS (Advanced Materials, Structures and Technologies). Retrieved from www.admas.cz	30
4.2	Every year the 3D printing lab at AdMaS participates at a public event for public (Night of Science). Photographed by the author in 2018.	31
4.3	The structural testing laboratory within the Department of Civil Engineering and Natural Hazards, Institute of Structural Engineering (IKI), University of Natural Resources and Life Sciences, Vienna. Photographed by the author in 2018.	32
4.4	Kuka six-axis robot and additive manufacturing at StrojLab, which is part the Fab Lab global network. Retrieved from www.strojlab.cz	33
5.1	Example of classical design approach. Source: co-authored [22]	39
5.2	Topological optimization in IDEA StatiCa (Red parts are more utilized, blue parts are less utilized). Source: co-authored [22]	39
5.3	Optimised organic frame with variable density governed by bio-inspired 3D infill). Source: co-authored [22]	40
5.4	Classical topology optimization work-flow in Ansys Workbench 19.1. Figure by author.	41
5.5	Classical topology optimization principle: initially defined solid body with boundary conditions (left) and the retained 15% mass after iterative removal of least stressed elements. Figure by author.	41
5.6	Printouts of topology optimization results and fractal principle: element size governs the overall shape. Photographed by author in 2018.	42
5.7	Classical topology optimization beam example with two levels of retained mass (left 30%, right 15%) and uniformly distributed load (red) at the bottom face of the supported (blue) beam. Figure by author.	43
6.1	Detail of a branching structure and 3D infill (gyroid). Figure by author. . . .	46
6.2	Detail of a branching structure and 2D infill (hexagonal). Figure by author. .	47
6.3	Choices associated with 3D infills and multi-scale optimization: periodic implicit formulation (green), macro-scale characterization (orange), shell thickness (blue) and random/irregular components (red). Figure by author.	48
6.4	Principle of mapping local stress levels to infill thickness or scale. Figure by author.	49
6.5	Principle of multi-scale optimization: from outer shape (left), infill type (center) to infill wall composition(extruder travel moves and density). Figure by author.	50

7.1	Generated shapes (from upper left): (a) Gyroid, (b) Gyroid Squared R, (c) Gyroid Tripled, (d) Schwarz P, (e) Schwarz D, (f) Neovius. Source: co-authored [22]	52
7.2	LDPM models of classical concrete experiments and particle placement governed by gradient-based fields (a) and random fields (b). Figure by author.	54
7.3	Example of qualitatively different failure modes of LDPM models resulting from microstructural differences and governing random fields. Figure by author.	55
7.4	Two random LDPM realizations of 3PB experiments governed by the same random field model. Figure by author.	56
7.5	Experimental production and testing process of the Gyroid RVE. Figure by author.	57
7.6	Load-displacement diagram of the gyroid sample printed from PLA. Figure by author.	57
7.7	Gyroid sample printed from PLA after the compression test. Figure by author.	58
8.1	Overview of tested 3D and 2D infill alternatives (left to right): Schwarz P, Schwarz D, Gyroid and Hexagonal; and sizes (top to bottom): Large, Medium and Small. Figure by author.	62
8.2	Example of 3D printed 3D infill patterns (Schwarz P, Schwarz D and Gyroid at medium scale) generated inside a cylinder. Photographed by author in 2018.	63
9.1	Industrial grade large scale FDM 3D printer Builder 2000. Photographed by the author in 2018.	66
9.2	Desktop FDM 3D printer Prusa i3 MK2. Photographed by the author in 2018.	67
9.3	Detail of several first layers of gyroid specimen and for increased adhesion a solid bottom face with a brim. Photographed by the author in 2018.	68
9.4	Sample group of 3D printed specimens from the same filament batch, i.e. same source and storing conditions, in order to eliminate detrimental effects of material degradation and ageing. Photographed by the author in 2018.	69
9.5	Different slicing strategies of material characterization based on ISO tensile test specimens (Top: DB 00, center: DB 90 and bottom: DB Hy). Figure by author.	69
9.6	Hydraulic compression testing machine controlled by a prescribed displacement rate in combination with a 3D digital image correlation (DIC) system enabling to record full strain fields and objectively interpret the load-displacement diagrams and stiffness. Photographed by the author in 2018.	71
9.7	Detail of the hydraulic compression test setup and visible high-contrast random pattern applied to the compressed specimen's surface for automated and reliable shape measurements with DIC. Photographed by the author in 2018.	72
9.8	Sample realizations of cylinder compression tests with 3 scales of reference 2D honeycomb infill. Photographed by the author in 2018.	73
9.9	Sample realizations of cylinder compression tests with 3 scales of 3D gyroid infill. Photographed by the author in 2018.	74
9.10	Sample realizations of cylinder compression tests with 3 scales of 3D Schwarz D infill. Photographed by the author in 2018.	75
9.11	Sample realizations of cylinder compression tests with 3 scales of 3D Schwarz P infill. Photographed by the author in 2018.	76

9.12	Three realizations of ISO dogbone specimens sliced according to DB 00 after the tensile test. Photographed by the author in 2018.	77
9.13	Three realizations of ISO dogbone specimens sliced according to DB 90 after the tensile test. Photographed by the author in 2018.	78
9.14	Three realizations of ISO dogbone specimens sliced according to DB Hy after the tensile test. Photographed by the author in 2018.	79
10.1	Mechanical performance of tested lattices as a function of weight: stiffness and peak load capacity. Figure by author.	82
10.2	ShD M: illustration of sequential collapse using damage localisation based on 5 DIC strain fields (Lagrange, horizontal component, A to E) mapped to black and white photos of the compressed specimens. Figure by author.	83
10.3	ShD M: illustration of sequential collapse using Load-Displacement diagram and positions of 5 DIC strain fields (A to E) from (fig. 10.2). Figure by author.	83
10.4	Material characterization based on ISO tensile test specimens and 3 different slicing strategies for nonlinear material model. Figure by author.	84
10.5	Periodic strain fields from the preliminary FEM analysis and different load levels. Figure by author.	85
10.6	Vacuum coating of the gyroid surface without the cylindrical confinement jacket. Photographed by the author in 2018.	87

List of Tables

7.1	Equations of surveyed minimal periodic surfaces.	51
7.2	Input parameters of surveyed minimal periodic surfaces.	52
7.3	Calculated parameters of surveyed minimal periodic surfaces.	53
10.1	Production and testing process variability based on 3 identical Gyroid specimens (* coefficient of variation).	81

Nomenclature

3DP	Three Dimensional Printing
3PB	Three-Point Bending test
ABS	Acrylonitrile Butadiene Styrene
AI	Artificial Intelligence
AM	Additive Manufacturing
ASTM	American Society for Testing and Materials
BIM	Building Information Modelling, Building Information Model or Building Information Management
BJ	Binder Jetting
BOD	Building On Demand
CAD	Computer Aided Design
CAM	Computer Aided Manufacturing
CNC	Computer Numerically Controlled
DB	Dog Bone tensile specimen
DED	Direct Energy Deposition
DM	Digital Manufacturing
FDM	Fused Deposition Modeling
FEM	Finite Element Model
FFF	Fused filament fabrication, also known as FDM
HCP	Hardened Cement Paste
HPC	High Performance Concrete
ISO	International Organization for Standardization
LDPM	Lattice Discrete Particle Model
LENS	Laser Engineered Net Shaping
LOM	Laminated Object Manufacturing

MARS	Multiscale-multiphysics Analysis of the Response of Structures
ME	Material Extrusion
MJ	Material Jetting
ML	Machine Learning
PBF	Powder Bed Fusion
PC	Polycarbonate
PLA	Polylactic Acid
RVE	Representative Volume Element
SL	Sheet Lamination
SLA	Stereolithographic Apparatus
SLS	Selective Laser Sintering
STL	Standard Tessellation Language or Standard Triangle Language
TPMS	Triply Periodic Minimal Surfaces
VP	Vat Photopolymerization

About the author

Jan Podrouzek obtained a bachelors degree in civil engineering (2008) from Brno University of Technology, Czech Republic. His dissertation work looked at degradation modelling of concrete structures using cellular automata. He then completed an engineering masters diploma in 2010 at the same institute in Construction and Traffic Structures. This focused on degradation and reliability modelling of concrete bridges. During his masters studies, Jan worked on several research projects at the department of chemistry and at the department of structural mechanics. His work specialised on nonlinear modelling of concrete behaviour, durability and reliability of concrete structures and cellular automata simulations including the stochastic effects. Jan graduated from the Doctoral Programme on Water Resource Systems at The Centre for Water Resource Systems, Vienna University of Technology, in 2014. His doctoral dissertation was entitled "A contribution to computationally efficient structural reliability assessment." After his graduation, Jan has had the opportunity to develop a large scale 3D printing laboratory at the research center for advanced materials and structures (AdMaS), which is part of Brno University of Technology, where he is also involved as teaching and research assistant at the Institute of computer aided engineering and computer science and Institute of structural mechanics. Jan also maintains a long-lasting cooperation with University of Natural Resources and Life Sciences, which contributed to part of the presented thesis.